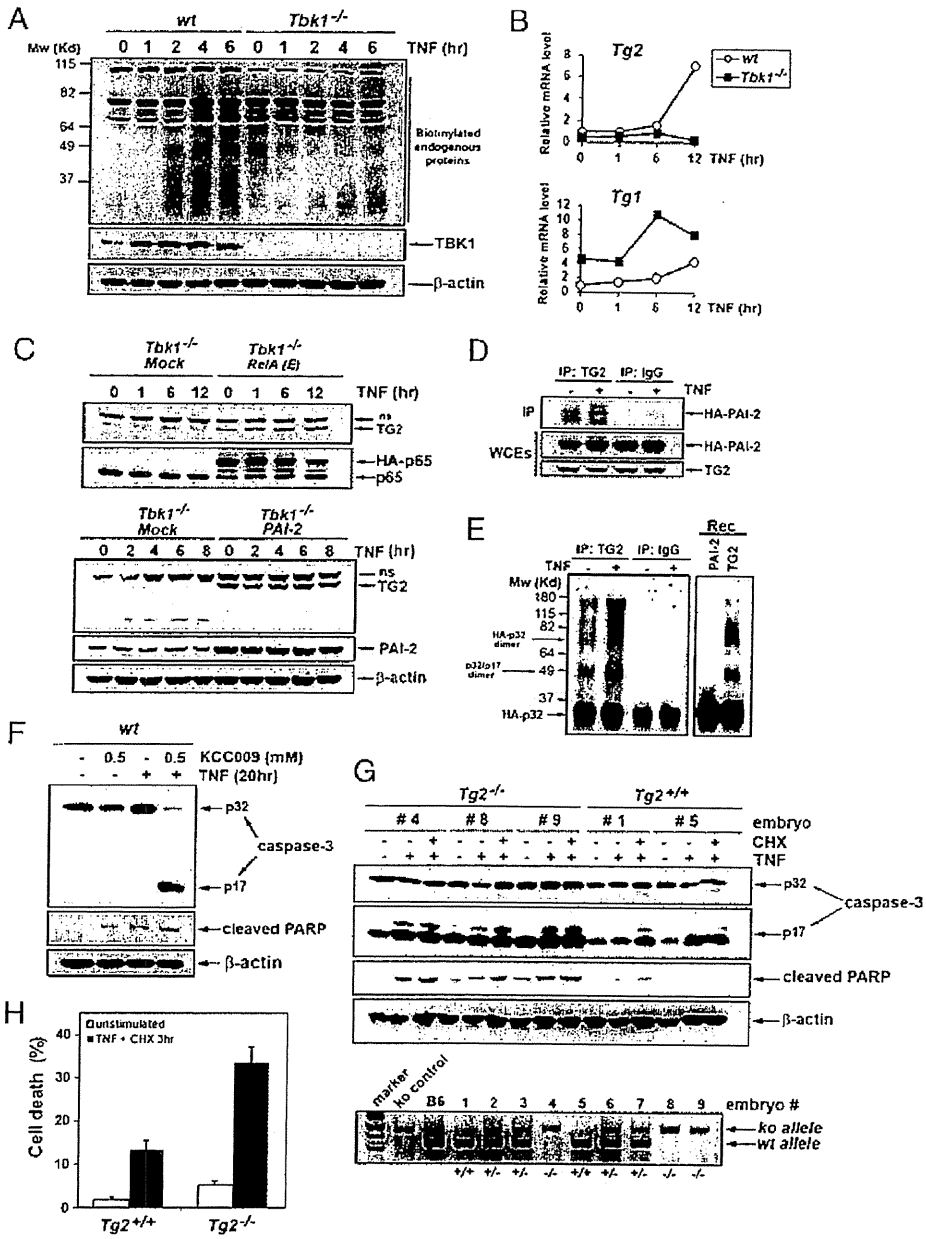

Fig. 4. TG2 is a TBK1-dependent antiapoptotic factor. (*A*) In vivo transamidation activity was determined in WT and *Tbk1*$^{-/-}$ MEFs metabolically labeled with BP and stimulated with TNF for the indicated times. Cell extracts were prepared, and biotin-conjugated proteins were detected by immunoblotting using anti-streptavidin-HRP (Pierce). (*B*) Induction of *Tg* gene expression was determined by qRT-PCR analysis of mRNAs from WT and *Tbk1*$^{-/-}$ MEFs stimulated with TNF for the indicated times. (*C*) Endogenous TG2 protein amounts were determined by immunoblotting in extracts from *Tbk1*$^{-/-}$ MEFs expressing RelA(E) (*Upper*), PAI-2 (*Lower*), or an "empty" retrovirus (mock) and treated with TNF for the indicated times (ns, nonspecific). (*D*) Coimmunoprecipitation of PAI-2 with TG2 was examined in MEFs stably expressing HA-PAI-2 and human TG2 that were left untreated or were stimulated with TNF for 8 h. Control immunoprecipitations were performed with nonimmune IgGs. (*E*) In vitro transamidation assay was performed with TG2 or control immunoprecipitates prepared from untreated or TNF-stimulated *Tbk1*$^{-/-}$ MEFs expressing TG2 and untagged PAI-2 or with recombinant proteins (rec) using HA-procaspase-3 as a substrate. (*F*) Wt MEFs were treated with TNF (20 h) with or without the transglutaminase-specific inhibitor KCC009 (0.5 mM). Caspase-3 activation, PARP cleavage, and protein expression were determined by immunoblotting. (*G*) WT and *Tg2*$^{-/-}$ primary MEFs prepared from littermate embryos were left untreated or treated with TNF alone (20 h) or TNF plus CHX (6 h). Caspase-3 activation and apoptosis were determined as detailed earlier. Genotyping (*Lower*) was performed by PCR amplification as described (31). (*H*) The extent of cell death in WT and *Tg2*$^{-/-}$ MEFs that were stimulated for 3 h with TNF plus CHX was quantified by staining with PI.

though TBK1 affects NF-κB target gene expression, it is not required for activation of NF-κB DNA binding (11). Early studies found TBK1 to form a complex with the adaptor molecules TRAF2 and TANK (8), which mediate assembly of signaling complexes at the intracellular tails of cytokine receptors (32). Indeed, TBK1 is recruited to TNFR1 upon TNF binding (10) and interacts with IKKγ/Nemo, the regulatory subunit of IKK (33, 34). We reported that TBK1 activates NF-κB through phosphorylation-mediated activation of the IKK complex (9). Consistent with a role for TBK1 in NF-κB signaling, *Tbk1*$^{-/-}$

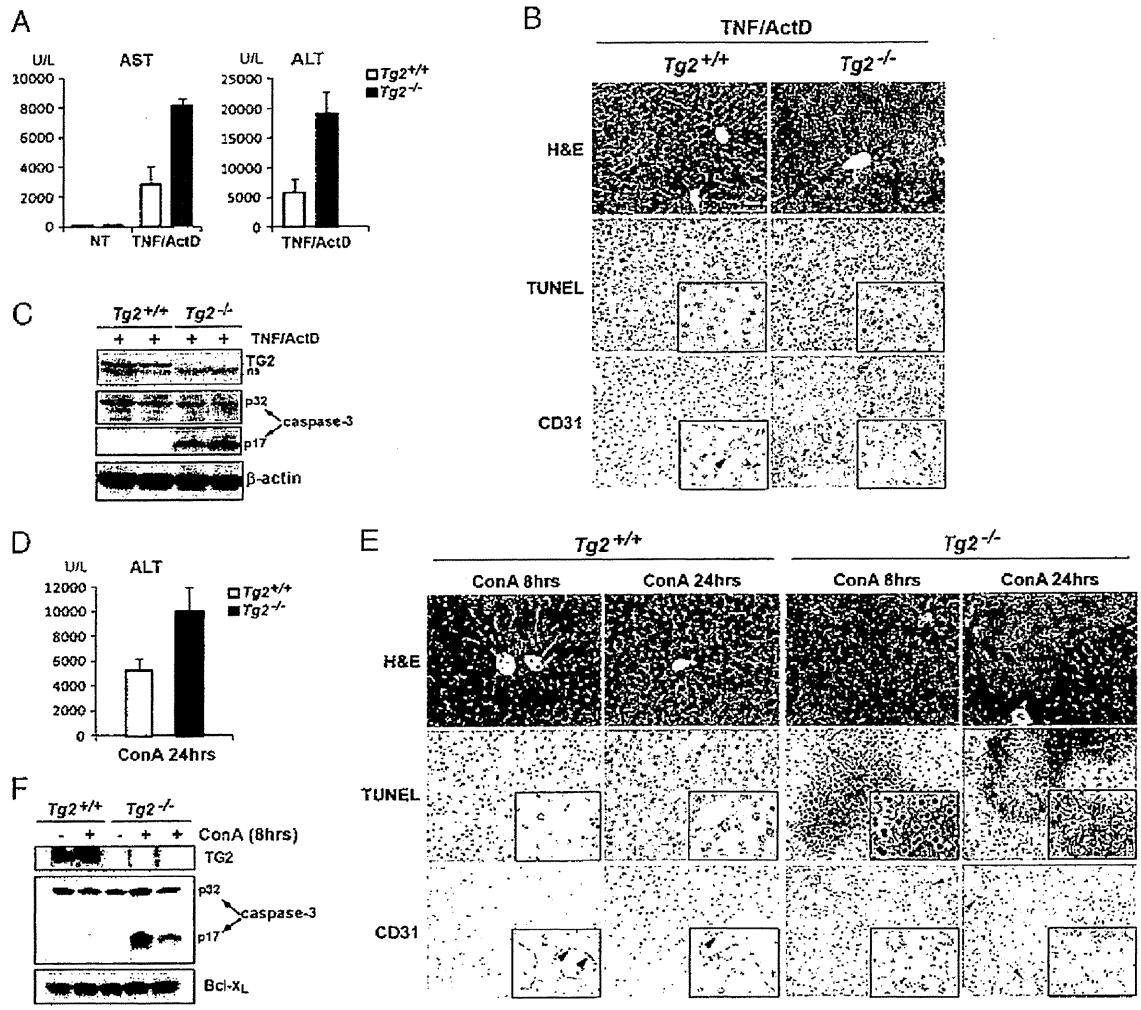

Fig. 5. TG2 protects mice from TNF-dependent liver apoptosis. (*A–C*) WT and $Tg2^{-/-}$ mice were injected with TNF and ActD and analyzed 16 h later. (*A*) Serum AST and ALT levels were determined in untreated mice (NT) or mice treated with TNF and Act D. Data are averages ± SD ($n = 3$). (*B*) Histological analysis (H&E staining), TUNEL staining, and anti-CD31 immunostaining were performed on sequential liver sections of WT and $Tg2^{-/-}$ mice 16 h after TNF and Act D injection. *Insets*: Higher magnification of a selected area. Arrowheads show vascular endothelial cells (CD31-positive), which are TUNEL-negative. CD31 immunostaining in $Tg2^{-/-}$ liver sections displayed some nonspecific background staining as a result of the presence of cell debris. (*C*) Caspase-3 activation was determined by immunoblot analysis of liver protein extracts prepared 16 h after TNF and Act D injection. (*D–F*) The same analyses were performed on WT and $Tg2^{-/-}$ at 8 h (*E* and *F*) or 24 h (*D* and *E*) after injection of Con A (35 mg/kg). (*D*) Serum AST and ALT levels measured after Con A injection. Data are averages ± SD ($n = 2$). (*E*) Histological analysis, TUNEL assays, and anti-CD31 staining were performed on sequential liver sections of WT and $Tg2^{-/-}$ mice at 8 h or 24 h after injection of Con A. *Insets*: Higher magnification of a selected area. TUNEL-positive cells (nuclear staining) in $Tg2^{-/-}$ liver sections are CD31-negative and represent apoptotic hepatocytes. Twenty-four hours of treatment with Con A induced massive liver degeneration in $Tg2^{-/-}$ mice, and dead cells were no longer detectable by TUNEL staining. Arrowheads point to vascular endothelial cells (CD31-positive cells), which are TUNEL-negative. (*F*) Liver extracts prepared from WT and $Tg2^{-/-}$ mice challenged with Con A (8 h) or PBS solution were analyzed for caspase-3 activation.

mice die during embryonic development from massive liver apoptosis and, like $Rela^{-/-}$, $Ikk\beta^{-/-}$, and $Ikk\gamma^{-/-}$ mice, they can be rescued by ablation of TNFR1 (11, 13). Cells derived from $Tbk1^{-/-}$ mice were reported to exhibit normal NF-κB activation without increased sensitivity to TNF-induced apoptosis (11). However, the present results show that TBK1 can directly phosphorylate RelA and thereby control the expression of a subset of NF-κB target genes that inhibit TNF-induced apoptosis. Our findings that $Tbk1^{-/-}$ MEFs are highly susceptible to TNF-induced apoptosis are consistent with the phenotype of $Tbk1^{-/-}$ fetuses, which exhibit all the characteristics of a defective TNF-induced and NF-κB–dependent antiapoptotic response (13). The divergence between our results and those reported earlier may result from different experimental conditions and detection methods. For instance, Bonnard et al. (11), examined cell viability by PI staining after stimulation of MEFs with a low dose of TNF (10 ng/mL), whereas we used a higher dose of TNF (25 ng/mL) without or with CHX and evaluated the apoptotic response by TUNEL assays and direct analysis of caspase-3 cleavage.

Molecular analysis of signaling events downstream of TNFR1 revealed that $Tbk1^{-/-}$ cells exhibit impaired IKK-mediated RelA phosphorylation at Ser^{534}, confirming the earlier suggestion that TBK1 modulates IKK activity (9). Importantly, expression of a phospho-mimic RelA(S534E) variant in $Tbk1^{-/-}$ MEFs restored the antiapoptotic response, demonstrating a specific biological function associated with RelA Ser^{534} phosphorylation, although this phosphorylation event is not critical for activation of most NF-κB target genes. These findings are consistent with previous reports that TNF-induced NF-κB activation is largely

normal in *Tbk1*$^{-/-}$ cells (11). Phosphorylation of RelA at Ser^{534} does not affect most RelA functions, including inhibition by IκBs, nuclear translocation, and binding to target gene promoters (Fig. S3). Instead, it modulates its ability to transactivate a specific subset of NF-κB target genes. Among these, we have identified *Pai-2* as a critical antiapoptotic gene and showed that reexpression of PAI-2 in *Tbk1*$^{-/-}$ MEFs inhibited the TNF-induced apoptotic response. Although NF-κB activation through induced IκB degradation is a well established signaling mechanism, it has long been suspected that expression of individual NF-κB target genes is further modulated through specific posttranslational modifications of NF-κB subunits (35, 36). We now show that one such mechanism involves RelA Ser^{534} phosphorylation, which depends on TBK1 and IKK activity. However, it is not yet clear how TBK1 directs IKK to specifically phosphorylate RelA Ser^{534} while having no effect on other IKK-dependent functions.

We also do not understand what causes the initial activation of caspase-8 in *Tbk1*$^{-/-}$ cells and how PAI-2 affects caspase-8 activation. We showed that cFLIP$_L$ is cleaved in a caspase-dependent manner when *Tbk1*$^{-/-}$ MEFs are stimulated with TNF in the presence of CHX (Fig. S1), and this may prompt initiation of the proapoptotic cascade. This is consistent with previous studies reporting that TNF promotes caspase-8 activation by elimination of cFLIP$_L$ when NF-κB–mediated *cFlip* induction is defective (5), de novo protein synthesis is blocked (37), or cFLIP degradation is enhanced (38). Furthermore, it was recently proposed that, in response to death receptor ligation, cFLIP and caspase-8 could form catalytically inactive heterodimers, which prevent the initiation of apoptosis (39).

Our results suggest that PAI-2 exerts its antiapoptotic function through interaction with and stabilization of TG2, which prevents caspase-3 activation by cross-linking of procaspase-3. Although it remains to be determined whether TG2 can also cross-link other caspases, including caspase-8, this observation provides a missing molecular link that explains the observation made more than a decade ago that the C-D interhelical domain or C-D loop of PAI-2, a conserved protein binding domain among ov-serpin family members (14), was essential for the antiapoptotic function of PAI-2 in TNF-stimulated cells (22). It was postulated that an interaction between the C-D loop and unknown proteins was likely to be important for resistance to apoptosis. We now show that PAI-2 interacts with TG2 in a TNF-dependent manner. This interaction presumably protects TG2 from proteolysis allowing TG2 to cross-link procaspase-3 and promote cell survival. Interestingly, another ubiquitously expressed ov-serpin family member, serpinB10 (PI10), was also found to provide protection against TNF-induced apoptosis (40). The authors observed the formation of high molecular weight SDS-stable PI10-containing complexes in cells treated with TNF in the presence of CHX (40). These complexes were suggested to contain a serine protease that is activated during this process, but this activity was never identified. Nevertheless, these observations raise the hypothesis that some ov-serpins may share a common function in controlling cell death, and that their specific physiological roles may have been obscured as a result of redundancy (14, 41). Although it remains to be further investigated, our observations that PAI-2 and TG2 interact in cells, and mediate a common antiapoptotic response, suggest that these unconventional antiapoptotic factors participate in a posttranslational mechanism that controls caspase-3 activation. Identification of the mechanism that controls TG2 turnover will provide additional insights into this antiapoptotic process.

The tumor suppressor retinoblastoma protein (Rb) is another intracellular target of PAI-2, which protects Rb from cleavage by calpains and thereby contributes to tumor cell survival (42). It was also shown that TG2 could protect Rb from caspase-7–mediated cleavage in fibroblasts (43). In light of our present results, it is tempting to speculate that PAI-2 and TG2 or a related enzyme may also control Rb-dependent cell survival. Notably, PAI-2 was also found to protect macrophages from pathogen-induced cell death (44), acting as a modulator of the innate immune response (45).

The antiapoptotic function of TG2 has been widely debated (25, 46), primarily because no spontaneous cell death was observed in *Tg2*$^{-/-}$ mice (31, 47, 48). However, TG2 protects cancer cells from thapsigargin- or hypoxia-induced death (23, 24), as well as staurosporine-induced apoptosis (49). Initial evidence for the antiapoptotic function of TG2 in vivo came from the work of Sarang et al. (26), who showed that *Tg2*$^{-/-}$ mice were more susceptible to Fas-mediated cell death. We now show in two different models of liver injury triggered by injection of TNF to Act D-sensitized mice or by Con A administration that *Tg2*$^{-/-}$ mice display increased hepatocyte apoptosis relative to WT counterparts (Fig. 5). These data strongly support a role for TG2 in inhibition of cell death mediated by members of the TNF/TNFR1 superfamily. However, an important question that needs to be answered is why *Pai-2*$^{-/-}$ and *Tg2*$^{-/-}$ mice are viable whereas genetic ablation of *Tbk1* leads to embryonic lethality. It could be argued that the newly identified PAI-2 and TG2-dependent pathway is not the only way by which TBK1 inhibits cell death. In addition, PAI-2 may act redundantly with PI10, as mentioned earlier. Furthermore, *Pai-2* is only one of several NF-κB–regulated antiapoptotic genes, such as *cIaps*, *cFlip*, *Bcl-X$_L$*, and others (5, 20), whose expression is needed to suppress TNF-induced liver destruction. Although the antiapoptotic function of these genes has never been disputed, genetic ablation of each one of them in isolation does not result in embryonic lethality as a result of liver failure. The current challenge is to identify the minimal set of antiapoptotic genes that needs to be expressed at a given time and in a particular environmental context during liver development and adult life to suppress TNF-driven hepatocyte death. It will also be interesting to test whether the combined ablation of both *Pai-2* and *Tg2* will result in a more severe phenotype that approaches that of *Tbk1*$^{-/-}$ mice. The identification of additional antiapoptotic factors whose expression or activity depends on TBK1 will shed further light on this question. Such factors may act independently of or in conjunction with the PAI-2–TG2 pathway.

Materials and Methods

Reagents. CHX, puromycin, z-VAD-FMK, MG-132, and protease inhibitors were from Calbiochem, and Act D, Con A, AEBSF, and Polybrene were from Sigma-Aldrich. Recombinant human PAI-2 was from Peprotech. Antibodies against RelA/p65 (S536) (no. 3031), phospho-IκBα (no. 9241), phospho-MAPKs (no. 9910), phospho-cJun (no. 9261), ERK, p38 (no. 9212), TBK1 (no. 3012), Bcl-X$_L$ (no. 2764), c-IAP1 (no. 4952), mBID (no. 2003), caspase-3 (no. 9662), cleaved caspase-3 (no. 9661), and cleaved PARP (no. 9544) were from Cell Signaling; antibodies to IKKγ (no. 557383), JNK1 (no. 551196), XIAP (no. 610716), CD95/Fas receptor (554254), caspase-8 (no. 559932), and procaspase-3 (no. 65906E) were from BD Transduction Laboratories; antibodies to IKKα (no. IMG-136A), IKKβ (no. IMG-129A), TBK1 (IMG-139A), and IκBα (no. IMG-127A) were from Imgenex; antibodies against RelA (sc-372 and sc-372-G), RelB, cRel, IκBβ, HSP60, and PAI-2 (sc-25746) were from Santa Cruz Biotechnology; anti-p65/RelA (CT), anti–phospho-ATF-2 (no. 05–891), anti-TG2 (no. 06–471), and anti-caspase-1 (no. 06–503) were from Upstate Biotechnology; anti–CREB-1 (AB3006) was from Millipore; anti-FLIPα (CT; no. 1161) was from ProSci, anti-TG2 (AB-4) was from Neomarkers (Lab Vision), anti-HA (clone 3F10) was from Roche, anti-cAIP2 was from R&D Systems, and anti-CD31 was from Abcam.

Immunoblotting. Whole-cell extracts were obtained by lysing cells in a buffer containing 50 mM Tris-HCl, pH 7.6, 250 mM NaCl, 1% Triton X-100, 0.5% Nonidet P-40, 3 mM EDTA, 3 mM EGTA, 10% glycerol, 2 mM DTT, 1 mM PMSF, 1 mM sodium orthovanadate, and a protease inhibitor mixture (Calbiochem). Nuclear extracts were prepared using NE-PER Nuclear and Cytoplasmic Extraction Reagents (Pierce). Proteins were separated by SDS/PAGE and blotted onto PVDF membranes (Millipore). The membranes were probed with the

appropriate antibodies and the antigen–antibody complexes detected by SuperSignal Western Pico Luminol/Enhancer solution (Pierce).

Kinase Assays. The IKK complex was immunoprecipitated from cell extracts using an anti-IKKγ antibody and the IKK activity was measured by in vitro kinase assay as described (19, 50) by using GST-IκBα(1-54) or GST-p65(354-551) as substrates.

Phosphorus-32 Metabolic Labeling and Phospho-Peptide Mapping. Cells were labeled with [^{32}P]orthophosphate as previously described (19, 50). Briefly, cells incubated with [^{32}P]orthophosphate (2 mCi/mL) for 5 h were stimulated with TNF (25 ng/mL) for 15 min, washed with PBS solution, and harvested in RIPA buffer. RelA was immunoprecipitated from precleared lysates by using an anti-RelA/p65 antibody (C-20; Santa Cruz Biotechnology). Immune complexes were washed in RIPA buffer. The proteins were resolved by SDS/PAGE and transferred to PVDF membranes (Millipore) for autoradiography and immunoblot analysis. Phospho-peptide mapping of phospho-labeled RelA/p65 was performed as described (19, 50).

Site-Directed Mutagenesis. Site-directed mutagenesis was performed using the Quick Exchange Mutagenesis kit (Stratagene) according to the manufacturer's instructions.

Retroviral Transductions. cDNAs were subcloned into the pLPCX retroviral vector (Stratagene). Recombinant retroviruses were produced by cotransfection with pCL-Eco into Phoenix packaging cells using Lipofectamine Plus reagent (Invitrogen). Supernatants containing recombinant retroviruses were collected 2 d after transfection, filtered to remove cell debris, and used directly for infection. MEFs at subconfluence were infected with viral stocks in the presence of Polybrene at 8 μg/mL, and two or three consecutive infections were performed over a period of 24 h. One day after the last infection, the infected cells were selected in medium supplemented with 2 μg/mL puromycin. Experiments were performed with pools of stable cells.

Gene Silencing Using shRNAs. Retroviral vectors (pRS plasmids) encoding shRNAs specific to mPAI-2 or a scrambled shRNA were purchased from Origene. Production of retroviruses, infection of cells and selection of stable cells were performed as described earlier. The most efficient *Pai-2*–specific shRNA construct among four tested was used.

Apoptosis Assays. Cells gown on Permanox Lab-Tek chamber slides were left untreated or stimulated with TNF (25 ng/mL) in the presence or absence of CHX (10 μg/mL) for the indicated times. Cells were fixed with 4% paraformaldehyde and permeabilized for 5 min with 0.1% Triton X-100 in 0.1% sodium citrate at 4 °C. Apoptotic cells were detected by TUNEL staining (Roche or Promega). DAPI staining was performed for total cell counting.

Immunofluorescence. Cells cultured on Lab-Tek chamber slides were left untreated or stimulated for 30 min with TNF (25 ng/mL). Cells were fixed with 4% paraformaldehyde, and the subcellular localization of RelA/p65 was examined by fluorescent immunostaining by using a polyclonal antibody against p65 (C-20) and Alexa-labeled anti-rabbit purified IgG (Jackson ImmunoResearch).

qRT-PCR and Microarray Analysis. Total RNA was extracted using TRIzol LS (Invitrogen) and purified on RNeasy Miniprep columns (Qiagen). For qRT-PCR analysis, cDNAs were synthesized by using a SuperScript II cDNA synthesis kit (Invitrogen). Real-time PCR amplifications were performed in 96-well optical reaction plates with Power SYBR Green PCR Master Mix (Applied Biosystems). Primers were designed by using Primer Express software. Primer sequences are available upon request. For microarray analysis, preparation of cDNA probes, hybridization to a mouse 10k oligo DNA microarray, scanning of the microarrays, and data analysis were performed by the Nippon Laser and Electronics Lab (Nagoya, Japan).

ChIP Assays. ChIP assays were performed as described (51) by using a polyclonal antibody against RelA/p65 (C-20; Santa Cruz Biotechnology). Samples were analyzed by PCR. Sequence information of the promoter-specific primers is available upon request.

In Vivo Transamidation. Assays were performed essentially as described previously (27). Cells were metabolically labeled with 1 mM pentylamine-biotin (BP; Pierce) added to the culture medium for 1 h before stimulation with TNF (25 ng/mL) for the indicated times. Cells were washed with PBS solution and harvested, and cell extracts were prepared by sonication in urea-containing buffer (50 mM Tris HCl, pH 7.6, 250 mM NaCl, 2 M urea, 0.05% SDS, 40 mM DTT, and a protease inhibitor mixture). Proteins were resolved by SDS/PAGE (10% gel) and transferred onto nitrocellulose membranes (Schleicher and Schuell), and proteins that incorporated BP were detected by using HRP-conjugated streptavidin and chemiluminescence (Pierce).

In Vitro Transamidation Assays. The mouse procaspase-3 cDNA was HA-tagged and subcloned into pBluescript KS(+) (Stratagene). The protein was expressed by in vitro coupled transcription-translation in reticulocyte lysate (Promega), immunoprecipitated with anti-HA beads (Roche), and eluted with HA-peptide. The protein was further incubated with PAI-2 or TG2 immunoprecipitated from cell extracts or with recombinant proteins in a buffer containing 50 mM Tris HCl, pH 8.5, 150 mM NaCl, 5 mM $CaCl_2$, and a protease inhibitor mixture (Calbiochem). The reactions were carried out for 1 h at 37 °C. HA-tagged procaspase-3 was detected by SDS/PAGE and immunoblotting using anti-HA or anti–procaspase-3 antibodies.

Mice. *Tg2*$^{-/-}$ mice were generated by homologous recombination (31) and were back-crossed to C57BL/6 mice for more than eight generations.

Preparation of MEFs. MEFs were prepared from individual littermate embryos at embryonic day 13.5 by using a standard procedure. Briefly, after removal of the head and the liver, the embryonic tissue was washed twice with PBS solution and treated with trypsin/EDTA for 30 min. The homogenates were transferred into a 150-mm dish containing complete culture medium (DMEM supplemented with 10% FBS, 0.1 mM β-mercaptoethanol, and antibiotics). Cells were passaged every 2 to 3 d. Experiments were performed with cells at passages three and four. The genotype of MEFS was determined and confirmed by PCR using genomic DNA extracted from yolk sac and MEFs.

Liver Injury Models. All experimental protocols were conducted in accordance with the Korean law on animal protection and approved by the institutional animal care and use committee at the National Cancer Center of Korea. Mice (9–10 wk old) were injected intraperitoneally with 20 μg of Act D and 0.3 μg of mouse TNF (no.575202; Biolegend). Alternatively, Con A was injected through the tail vein at 35 mg/kg. In both cases, PBS solution was injected in control animals. Mice were killed 8 h, 24 h (Con A), or 16 h (TNF and Act D) after challenge. Blood was collected by cardiac puncture, and the livers were surgically removed. Serum ALT and AST levels were determined by using Fuji Dri-Chem Slides AST-/ALT-PIII (FujiFilm) according to the manufacturer's instructions. Liver tissue samples were fixed in 10% buffered formalin and processed for paraffin embedding and histological evaluation. Pieces of liver tissue were snap-frozen and used for preparation of whole-liver protein extracts. Histological analysis was performed on liver sections (2–3 μm thick) after routine H&E staining. In situ TUNEL assays were performed on tissue sections by using an in situ apoptosis detection kit (Takara Bio) according to the manufacturer's instructions. Briefly, deparaffinized sections were treated with proteinase K and washed with PBS solution, and endogenous peroxidase activity was inactivated in 3% H_2O_2. After terminal-deoxynucleotidyl transferase enzymatic reaction, the signal was detected by using an HRP-labeled anti-FITC antibody and visualized with DAB as substrate.

Immunohistochemistry. Deparaffinized tissue sections were incubated with anti-CD31 (PECAM-1; Abcam) at a dilution of 1:50. Antibody binding was detected by using a HRP-linked secondary antibody and revealed by conventional immunostaining performed in an autoimmunostaining apparatus (HX System; Ventana) using DAB as substrate.

ACKNOWLEDGMENTS. We thank D. Rothwarf for critical reading of the manuscript and helpful suggestions; W.-C. Yeh, S. Akira, A. Beg, A. Hoffmann, R. Flavell, and Z.-W. Li for providing *Tbk1*$^{-/-}$, *RelA/p65*$^{-/-}$, *IκBα*$^{-/-}$, *caspase-3*$^{-/-}$, and *Ikkαlβ*$^{-/-}$ MEFs, respectively; P. Brouckaert for providing mTNF; M. Hernandez (Applied Biosystems) for advice on quantitative PCR; C. H. Jeon for technical assistance; and D. Ginsburg, M. Montminy, T. Kato, and S. Imajoh-Ohmi for plasmids and antibodies. M.D. was supported by a grant from the Claudia Adams Barr Program in Cancer Research. K.S.K. was supported by the National Institutes of Health (NIH). This work was supported by National Cancer Center (Korea) Research Grants NCC 0510270 and NCC1110011-1 (to H.L. and S-Y.K.), National Research Foundation Grant 2010-0029919 funded by the Korean government (to S-Y.K.), NIH Grant AI043477 (to M.K.), and Grants-in-Aid for Scientific Research on Priority Area and for Scientific Research (B) by the Ministry of Education, Science, Sports, and Culture of Japan (M.N.), M.K. is an American Cancer Society Research Professor.

1. Green DR, Evan GI (2002) A matter of life and death. *Cancer Cell* 1:19–30.
2. Li J, Yuan J (2008) Caspases in apoptosis and beyond. *Oncogene* 27:6194–6206.
3. Chen G, Goeddel DV (2002) TNF-R1 signaling: A beautiful pathway. *Science* 296: 1634–1635.
4. Wajant H, Scheurich P (2011) TNFR1-induced activation of the classical NF-κB pathway. *FEBS J* 278:862–876.
5. Karin M, Lin A (2002) NF-kappaB at the crossroads of life and death. *Nat Immunol* 3: 221–227.
6. Burstein E, Duckett CS (2003) Dying for NF-kappaB? Control of cell death by transcriptional regulation of the apoptotic machinery. *Curr Opin Cell Biol* 15:732–737.
7. Janes KA, et al. (2006) The response of human epithelial cells to TNF involves an inducible autocrine cascade. *Cell* 124:1225–1239.
8. Pomerantz JL, Baltimore D (1999) NF-kappaB activation by a signaling complex containing TRAF2, TANK and TBK1, a novel IKK-related kinase. *EMBO J* 18:6694–6704.
9. Tojima Y, et al. (2000) NAK is an IkappaB kinase-activating kinase. *Nature* 404: 778–782.
10. Kuai J, et al. (2004) NAK is recruited to the TNFR1 complex in a TNFalpha-dependent manner and mediates the production of RANTES: identification of endogenous TNFR-interacting proteins by a proteomic approach. *J Biol Chem* 279:53266–53271.
11. Bonnard M, et al. (2000) Deficiency of T2K leads to apoptotic liver degeneration and impaired NF-kappaB-dependent gene transcription. *EMBO J* 19:4976–4985.
12. Hemmi H, et al. (2004) The roles of two IkappaB kinase-related kinases in lipopolysaccharide and double stranded RNA signaling and viral infection. *J Exp Med* 199:1641–1650.
13. Gerondakis S, et al. (2006) Unravelling the complexities of the NF-kappaB signalling pathway using mouse knockout and transgenic models. *Oncogene* 25:6781–6799.
14. Izuhara K, Ohta S, Kanaji S, Shiraishi H, Arima K (2008) Recent progress in understanding the diversity of the human ov-serpin/clade B serpin family. *Cell Mol Life Sci* 65:2541–2553.
15. Liu ZG, Hsu H, Goeddel DV, Karin M (1996) Dissection of TNF receptor 1 effector functions: JNK activation is not linked to apoptosis while NF-kappaB activation prevents cell death. *Cell* 87:565–576.
16. Tang G, et al. (2001) Inhibition of JNK activation through NF-kappaB target genes. *Nature* 414:313–317.
17. Fujita F, et al. (2003) Identification of NAP1, a regulatory subunit of IkappaB kinase-related kinases that potentiates NF-kappaB signaling. *Mol Cell Biol* 23:7780–7793.
18. Buss H, et al. (2004) Constitutive and interleukin-1-inducible phosphorylation of p65 NF-kappaB at serine 536 is mediated by multiple protein kinases including IkappaB kinase (IKK)-alpha, IKKbeta, IKKepsilon, TRAF family member-associated (TANK)-binding kinase 1 (TBK1), and an unknown kinase and couples p65 to TATA-binding protein-associated factor II31-mediated interleukin-8 transcription. *J Biol Chem* 279: 55633–55643.
19. Delhase M, Hayakawa M, Chen Y, Karin M (1999) Positive and negative regulation of IkappaB kinase activity through IKKbeta subunit phosphorylation. *Science* 284: 309–313.
20. Pahl HL (1999) Activators and target genes of Rel/NF-kappaB transcription factors. *Oncogene* 18:6853–6866.
21. Kumar S, Baglioni C (1991) Protection from tumor necrosis factor-mediated cytolysis by overexpression of plasminogen activator inhibitor type-2. *J Biol Chem* 266: 20960–20964.
22. Dickinson JL, Norris BJ, Jensen PH, Antalis TM (1998) The C-D interhelical domain of the serpin plasminogen activator inhibitor-type 2 is required for protection from TNF-alpha induced apoptosis. *Cell Death Differ* 5:163–171.
23. Yamaguchi H, Wang HG (2006) Tissue transglutaminase serves as an inhibitor of apoptosis by cross-linking caspase 3 in thapsigargin-treated cells. *Mol Cell Biol* 26: 569–579.
24. Jang GY, et al. (2010) Transglutaminase 2 suppresses apoptosis by modulating caspase 3 and NF-kappaB activity in hypoxic tumor cells. *Oncogene* 29:356–367.
25. Lorand L, Graham RM (2003) Transglutaminases: Crosslinking enzymes with pleiotropic functions. *Nat Rev Mol Cell Biol* 4:140–156.
26. Sarang Z, et al. (2005) Tissue transglutaminase (TG2) acting as G protein protects hepatocytes against Fas-mediated cell death in mice. *Hepatology* 42:578–587.
27. Shin DM, et al. (2004) Cell type-specific activation of intracellular transglutaminase 2 by oxidative stress or ultraviolet irradiation: Implications of transglutaminase 2 in age-related cataractogenesis. *J Biol Chem* 279:15032–15039.
28. Lakhani SA, et al. (2006) Caspases 3 and 7: Key mediators of mitochondrial events of apoptosis. *Science* 311:847–851.
29. Masud A, et al. (2007) Endoplasmic reticulum stress-induced death of mouse embryonic fibroblasts requires the intrinsic pathway of apoptosis. *J Biol Chem* 282: 14132–14139.
30. Siegel M, Khosla C (2007) Transglutaminase 2 inhibitors and their therapeutic role in disease states. *Pharmacol Ther* 115:232–245.
31. Kim DS, et al. (2010) Transglutaminase 2 gene ablation protects against renal ischemic injury by blocking constant NF-κB activation. *Biochem Biophys Res Commun* 403: 479–484.
32. Napolitano G, Karin M (2010) Sphingolipids: The oil on the TRAFire that promotes inflammation. *Sci Signal* 3:pe34.
33. Chariot A, et al. (2002) Association of the adaptor TANK with the I kappa B kinase (IKK) regulator NEMO connects IKK complexes with IKK epsilon and TBK1 kinases. *J Biol Chem* 277:37029–37036.
34. Bouwmeester T, et al. (2004) A physical and functional map of the human TNF-alpha/NF-kappa B signal transduction pathway. *Nat Cell Biol* 6:97–105.
35. Ghosh S, Karin M (2002) Missing pieces in the NF-kappaB puzzle. *Cell* 109(suppl): S81–S96.
36. Perkins ND (2006) Post-translational modifications regulating the activity and function of the nuclear factor kappa B pathway. *Oncogene* 25:6717–6730.
37. Wang L, Du F, Wang X (2008) TNF-alpha induces two distinct caspase-8 activation pathways. *Cell* 133:693–703.
38. Chang L, et al. (2006) The E3 ubiquitin ligase itch couples JNK activation to TNFalpha-induced cell death by inducing c-FLIP(L) turnover. *Cell* 124:601–613.
39. Green DR, Oberst A, Dillon CP, Weinlich R, Salvesen GS (2011) RIPK-dependent necrosis and its regulation by caspases: A mystery in five acts. *Mol Cell* 44:9–16.
40. Schleef RR, Chuang TL (2000) Protease inhibitor 10 inhibits tumor necrosis factor alpha -induced cell death. Evidence for the formation of intracellular high M(r) protease inhibitor 10-containing complexes. *J Biol Chem* 275:26385–26389.
41. Dougherty KM, et al. (1999) The plasminogen activator inhibitor-2 gene is not required for normal murine development or survival. *Proc Natl Acad Sci USA* 96: 686–691.
42. Tonnetti L, et al. (2008) SerpinB2 protection of retinoblastoma protein from calpain enhances tumor cell survival. *Cancer Res* 68:5648–5657.
43. Boehm JE, Singh U, Combs C, Antonyak MA, Cerione RA (2002) Tissue transglutaminase protects against apoptosis by modifying the tumor suppressor protein p110 Rb. *J Biol Chem* 277:20127–20130.
44. Park JM, et al. (2005) Signaling pathways and genes that inhibit pathogen-induced macrophage apoptosis—CREB and NF-kappaB as key regulators. *Immunity* 23: 319–329.
45. Medcalf RL (2011) Plasminogen activator inhibitor type 2: Still an enigmatic serpin but a model for gene regulation. *Methods Enzymol* 499:105–134.
46. Fesus L, Piacentini M (2002) Transglutaminase 2: An enigmatic enzyme with diverse functions. *Trends Biochem Sci* 27:534–539.
47. De Laurenzi V, Melino G (2001) Gene disruption of tissue transglutaminase. *Mol Cell Biol* 21:148–155.
48. Nanda N, et al. (2001) Targeted inactivation of Gh/tissue transglutaminase II. *J Biol Chem* 276:20673–20678.
49. Rossin F, D'Eletto M, Macdonald D, Farrace MG, Piacentini M (2011) TG2 transamidating activity acts as a reostat controlling the interplay between apoptosis and autophagy. *Amino Acids*, 10.1007/s00726-011-0899-x.
50. Delhase M (2003) IkappaB kinase and NF-kappaB signaling in response to pro-inflammatory cytokines. *Methods Mol Biol* 225:7–17.
51. Saccani S, Pantano S, Natoli G (2002) p38-Dependent marking of inflammatory genes for increased NF-kappa B recruitment. *Nat Immunol* 3:69–75.

Genetic Variation of the IL-28B Promoter Affecting Gene Expression

Masaya Sugiyama[1,2,5], Yasuhito Tanaka[3], Takaji Wakita[4], Makoto Nakanishi[2], Masashi Mizokami[1]*

1 The Research Center for Hepatitis and Immunology, National Center for Global Health and Medicine, Ichikawa, Chiba, Japan, **2** Department of Biochemistry and Cell Biology, Nagoya City University Graduate School of Medical Sciences, Mizuho, Nagoya, Japan, **3** Department of Virology and Liver Unit, Nagoya City University Graduate School of Medical Sciences, Mizuho, Nagoya, Japan, **4** Department of Virology II, National Institute of Infectious Diseases, Shinjuku, Tokyo, Japan, **5** JSPS Research Fellow, Japan Society for the Promotion of Science, Chiyoda, Tokyo, Japan

Abstract

The current standard of care for the treatment of chronic hepatitis C is pegylated interferon-α (PEG-IFNα) and ribavirin (RBV). The treatment achieves a sustained viral clearance in only approximately 50% of patients. Recent whole genome association studies revealed that single nucleotide polymorphisms (SNPs) around *IL-28B* have been associated with response to the standard therapy and could predict treatment responses at approximately 80%. However, it is not clear which SNP is most informative because the genomic region containing significant SNPs shows strong linkage disequilibrium. We focused on SNPs in close proximity to the *IL-28B* gene to evaluate the function of each and identify the SNP affecting the *IL-28B* expression level most. The structures of *IL-28A/B* from 5′ to 3′-UTR were determined by complete cDNA cloning. Both *IL-28A* and *28B* genes consisted of 6 exons, differing from the CCDS data of NCBI. Two intron SNPs and a nonsynonymous SNP did not affect *IL-28B* gene function and expression levels but a SNP located in the proximal promoter region influenced gene expression. A (TA) dinucleotide repeat, rs72258881, located in the promoter region was discovered by our functional studies of the proximal SNPs upstream of *IL-28B*; the transcriptional activity of the promoter increased gradually in a $(TA)_n$ length-dependent manner following IFN-α and lipopolysaccharide stimulation. Healthy Japanese donors exhibited a broad range of (TA) dinucleotide repeat numbers from 10 to 18 and the most prevalent genotype was 12/12 (75%), differing from the database (13/13). However, genetic variation of *IL-28A* corresponding to that of *IL-28B* was not detected in these Japanese donors. These findings suggest that the dinucleotide repeat could be associated with the transcriptional activity of *IL-28B* as well as being a marker to improve the prediction of the response to interferon-based hepatitis C virus treatment.

Citation: Sugiyama M, Tanaka Y, Wakita T, Nakanishi M, Mizokami M (2011) Genetic Variation of the *IL-28B* Promoter Affecting Gene Expression. PLoS ONE 6(10): e26620. doi:10.1371/journal.pone.0026620

Editor: John E. Tavis, Saint Louis University, United States of America

Received June 29, 2011; **Accepted** September 29, 2011; **Published** October 25, 2011

Funding: This work was supported by a Grant-in-Aid from the Ministry of Health Labor and Welfare of Japan and a Grant-in-Aid from the Ministry of Education, Culture, Sports, Science, and Technology of Japan (271000) and The Grant of National Center for Global Health and Medicine (22–302). The funders had no role in study design, data collection and analysis, decision to publish, or preparation of the manuscript.

Competing Interests: The authors have declared that no competing interests exist.

* E-mail: mmizokami@hospk.ncgm.go.jp

Introduction

A novel group of cytokines was discovered simultaneously by two independent groups in 2003 and named interferon lambda (IFN-λ) [1,2] or type III IFN. Type III IFN comprises three members, IFN-λ1, 2, and 3 or *IL-29* and *IL-28A*, and *IL-28B*, respectively. Type III IFN is a member of the class II cytokine family. This family includes type I, II, and III interferons and the IL-10 family (IL-10, IL-19, IL20, IL-22, IL-24, and IL-26). IFN-λ uses a distinct receptor complex consisting of a unique subunit, named IFN-λR1, and the IL-10R2 subunit. Expression of the IFN-λR1 receptor subunit is highly restricted, whereas the type I IFN receptor complex and the IL-10R2 receptor were detected in most cell types [1,2,3,4,5,6]. The IL-10R2 receptor subunit is shared by IL-10, IL-22, IL-24, IL-26, and IFN-λ. This suggests that type III IFNs act in a rather cell-type specific manner to mediate their biological functions. Type III IFNs trigger a type I IFN-like gene expression profile [5,6,7], which has been shown to have antiviral activity *in vitro* and *in vivo* [1,2,5,6,8]. Thus, the two types of IFN seem to have similar biological effects at a cellular level. IFN-α and IL-29/28A treatment reduced the concentration of hepatitis C virus (HCV) plus-strand RNA in an *in vitro* assay [6,9,10,11]. In addition, IL-29 may have therapeutic value against chronic viral hepatitis in human patients [5].

Recently, a genome-wide association study (GWAS) revealed that several highly correlated common single nucleotide polymorphisms (SNPs), in a linkage disequilibrium (LD) block encompassing the *IL-28B* genes on chromosome 19q13, are implicated in the response of chronic hepatitis C (CHC) patients to pegylated IFN-alpha (PEG-IFNα) and ribavirin (RBV) [12,13,14]. The CC genotype of rs12979860 and TT genotype of rs8099917 are associated in CHC patients with a sustained viral response (SVR) of 2.5 or greater rate, which is dependent of ethnicity, compared to the other genotypes. Moreover, the CC genotype of rs12979860 and TT genotype of rs8099917 favor spontaneous clearance of HCV [15].

We have reported the genomic analysis of approximately 15 kb containing the significant SNPs using Haploview software for LD and haplotype structure [14,16]. To analyze the difference in LD pattern between races, we performed LD mapping with these SNPs on JPT (Japanese in Tokyo), CEU (Utah residents with ancestry from Northern and Western Europe) or YRI (Yoruba in

Ibada, Nigeria) populations. These SNPs were in strong LD in JPT and CEU populations, although relatively low LD was predicted in the YRI population [14,16], suggesting that any of the SNPs located in this region could be responsible for treatment response. Because of the strong LD, tests for independence among these variants were not able to reveal which of these SNPs is uniquely responsible for the association with virological response (VR) or non-virological response (NVR). The identification of the primary genetic variant located in the LD block remained critical, although the risk haplotype tended to influence the expression levels or activity of *IL-28B* [13,14]. In this study, we sought to determine the primary SNP affecting IL-28B expression and/or its function by focusing on the proximal regulatory region of *IL-28B*.

IL-28B was discovered as a member of the IFN-λ family by Sheppard et al. and Kotenko et al. [1,2]. They discovered this family, *IL-29*, *IL-28A*, and *IL-28B* and the specific receptor, *IL-28RI*, by applying individual computational techniques to the draft human genome. However, the start codon of IFN-λ differs between the reports, with an additional 12 nucleotides at the N-terminus in all IFN-λs reported by Sheppard et al. (Fig. S1). The sequence similarity between these ORFs is approximately 96.7% and, especially, there is a high degree of identity between *IL-28A* and *IL-28B* cDNA (approximately 98%). Figure 1A shows the locations of *IL-28A/B* gene, the significant SNPs around *IL-28B* related to anti-HCV therapy reported in previous studies [12,13,14], and $(TA)_n$ repeats in the regulatory region of *IL-28A* and *B*. The SNPs information assessed in this study is summarized in Table 1 and the locations of the SNPs are shown in the schematic of the *IL-28B* gene (Fig. 1B). The reference sequences of *IL-28A* or *IL-28B* cDNA, registered in NCBI CCDS, are composed of 6 exons and 5 exons, respectively (Fig. 1B). Because high sequence similarity was observed between *IL-28A* and *IL-28B* from CpG to the region downstream of 3′-UTR (Fig. S2), the genes were almost completely identical around transcription start site (TSS) (>99%). Then, we determined the likely gene structure using a complete cDNA cloning method because a similar transcriptional mechanism was expected for *IL-28A* and *IL-28B*.

Materials and Methods

Genome samples

Genome samples were obtained from 20 healthy volunteers (HV). Peripheral blood mononuclear cells (PBMC) collected from HV were isolated using the BD Vacutainer CPT Method (BD Biosciences). Genomic DNAs were extracted by standard methods. SNPs were selected from the database at GWAS database (https://gwas.lifesciencedb.jp/cgi-bin/gwasdb/gwas_top.cgi). Written informed consent was provided by all participants in the genotyping study following procedures approved by the Ethical Committee at Nagoya City University.

Cell lines

Human hepatocellular carcinoma cell lines, HepG2 and HuH7, human hepatocyte cell lines, HuSE2 (kindly provided by Dr. Hijikata in Kyoto University), and the human cervical cancer cell line, HeLa (obtained from The American Type Culture Collection), were cultured in Dulbecco's modified Eagle's medium supplemented with 10% (v/v) fetal bovine serum, 100 U ml^{-1} penicillin and 100 mg ml^{-1} streptomycin. Human leukemia virus type 1 transformed cell line, MT-2 (a gift from Dr. Ueda in Nagoya City University), Burkitt lymphoma cell line, Raji, and human T cell leukemia cell line, Jurkat (obtained from The American Type Culture Collection), were cultured in RPMI 1640 medium supplemented with 10% (v/v) fetal bovine serum, 100 U ml^{-1} penicillin and 100 mg ml^{-1} streptomycin. All incubations were performed at 37°C in a 5% CO_2 gassed incubator. Recombinant human IFN-λ2 and -3 were purchased from R&D Systems (Abingdon, UK). Natural human IFN-α was

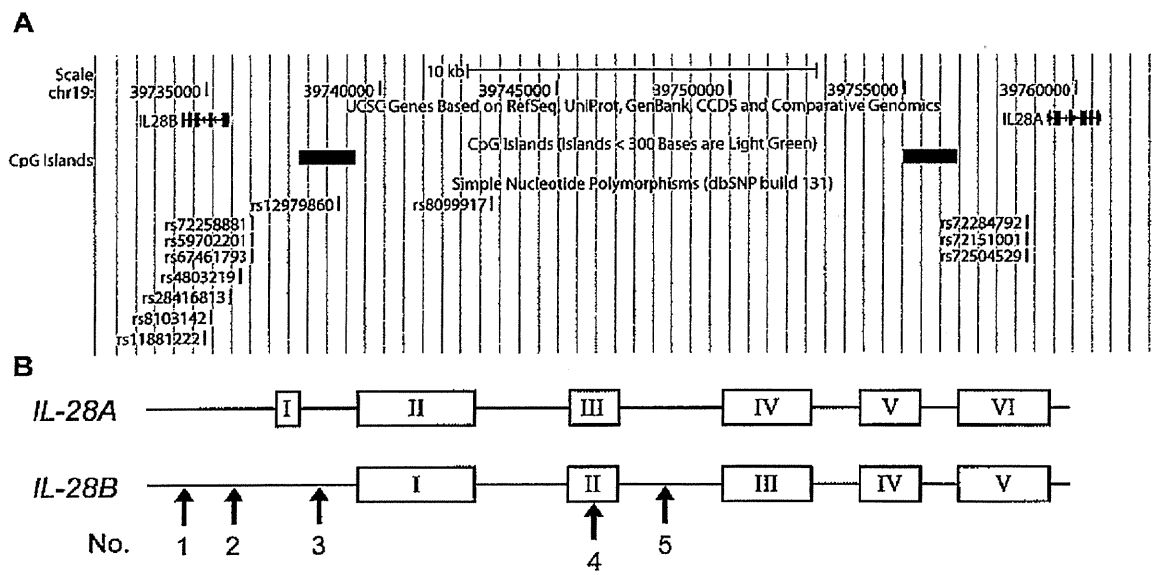

Figure 1. The position of significant SNPs and IL-28A/B in chromosome 19, retrieved from the database. (A) The *IL-28A/B* genes located in chromosome 19q13 are described in the genome map of the UCSC genome browser. The significant proximal SNPs around *IL-28B* associated with response to PEG-IFN/RBV therapy are shown in the map [14]. SNPs of $(TA)_n$ variation at the regulatory region of *IL-28A* are displayed in the position corresponding to that of *IL-28B*, which is not associated with anti-HCV therapy. (B) The schematic of *IL-28A/B* gene structure is described based NCBI CCDS data. Arrows show five significant SNPs examined in this study (see Table 1).
doi:10.1371/journal.pone.0026620.g001

Table 1. Significant SNPs around *IL-28B*.

Feature	rs ID	Allele 1/2*[1]	Minus strand*[2]	Location	No.
DIP*[3]	rs72258881*[4]	ATAT/-	TATA/-	Regulatory	1
Substitution	rs4803219	C/T	G/A	Regulatory	2
	rs28416813	C/G	G/C	Intron	3
	rs8103142	T/C	A/G	Nonsynonymous	4
	rs11881222	A/G	T/C	Intron	5

*[1]These data were derived from dbSNP. Allele 2 is the risk allele of HCV therapy reported by Tanaka *et al.*, except for rs72258881.
*[2]Complementary nucleotides are shown because *IL-28B* is coded on the minus strand.
*[3]DIP: deletion/insertion polymorphism.
*[4]The ID represents rs72258881, rs59702201, and rs67461793 because these three are located in the same genomic region, the TA repeat.
doi:10.1371/journal.pone.0026620.t001

purchased from Hayashibara co. ltd. (Okayama, Japan). The mRNA expression levels of receptors stimulated in this study were confirmed by PCR using gene specific primer (Table S1 and Fig. S3),

Plasmid Construction

As a T/G heterozygote genome of rs8099917 with a strong LD was used as the PCR template, amplicons from the major and minor alleles were obtained for the assay described below. PCR was carried out to amplify the fragment from −858 nt of the ATG site to TGA of *IL-28B*, and the products were inserted into pcDNA3.1/Hyg (pcDNA/MA or mi) or pcDNA3.1/Hyg vector deleting CMV promoter (pdCMV/MA or mi). A FLAG sequence was conjugated to 6th exon, removing the stop codon, for real time PCR analysis. The promoter region from nucleotide position −858 to +30 of *IL-28B* was amplified using pdCMV/MA or mi vector and inserted into pGL4 vector for the luciferase assay. A vector with an antisense insert was prepared as a control. For expression constructs, the wild type (WT) plasmids, pcDNA3.1/wild expressing human IL-28B, and pcDNA3.1/ns-mut expressing human IL-28B harboring a K^{74}R mutation, were generated using pcDNA3.1/V5-His-TOPO® (Invitrogen, San Diego, CA) and were used in the subsequent transfections. In addition, pcDNA3.1/AS expressing antisense strand of IL-28B was constructed as a control. We also obtained a pISRE-luc plasmid (provided by Sakamoto N., Tokyo Medical Dental University, Tokyo, Japan). The pGL4.74 vector encoding Renilla Luciferase was purchased from Promega (Madison, WI). These primer sequences are available on request. The above expression vectors were modified for the analysis of splicing function by introducing two intron SNPs (rs28416813 and rs11881222) (Table 1), which were pcDNA/WT, d-iSNPs.

Transient transfections

Transient transfections of HeLa, Jurkat, Raji, HuH7, HepG2, or HuSE2 (hepatocellular carcinomas cell line) cells were carried out using FuGene HD (Roche) or the Cell Line Nucleofector kit (Amaxa Biosystems) according to the manufacturers' protocols. Briefly, Cells (2×10^5) were seeded into a 6 well plate and transfected with for FuGene HD. For the electroporation method, cells (1.0×10^6) were collected and resuspended in Nucleofector solution V for each individual transfection sample.

5′-, 3′-RACE based on full-length cDNA cloning

Total RNA was prepared from cell lines stimulated with lipopolysaccharide (LPS) (0127:B8, Sigma-Aldrich) for 4 hours after 100 U/mL of IFN-α for 16 hours by following previous paper [17]. A GeneRacer Kit (Invitrogen Life Technologies) was used to obtain the complete cDNA sequence of *IL-28A/B* following manufacturer's instructions. Briefly, the GeneRacer RNA Oligo was ligated to the 5′ end specifically of full-length mRNA within the total RNA mixture. This ligated mRNA was then converted to cDNA using reverse transcriptase (RT) and the GeneRacer Oligo dT Primer. Next, this cDNA was used for PCR using the oligonucleotides of GeneRacer 5′ Primer and P1 primer which hybridized to the coding strand of the *IL28A/B* (Table S1). The resulting PCR products were then used for a second round of PCR using the oligonucleotides GeneRacer 5′ Nested Primer, which represents the DNA equivalent of the 3′ end of the GeneRacer RNA Oligo, and P2, which hybridizes to the coding strand of the *IL-28A/B* 5′ to the P1 hybridization site. For 3′ RACE, the cDNA was subjected to the polymerase chain reaction (PCR) to amplify the 3′ end using a forward gene-specific primer P3 designed from *IL-28A/B* and the GeneRacer 3′ primer provided with the kit. Nested PCR, using the same gene-specific primer and GeneRacer 3′ nested primer, was performed. The PCR product of 5′ and 3′ RACE was cloned into pCR4-TOPO TA vector according to the manufacturer's instructions (Invitrogen). Ten clones were isolated and subjected to automated sequencing (ABI3100, ABI) in our core facility.

Protein expression and purification

Recombinant IL-28B and its mutant were produced by transfecting Free-Style™ 293-F cells (purchased from Invitrogen, Carlsbad, CA) with the expression plasmid, which was grown in 5000 ml of FreeStyle 293 Expression Medium, following the manufacturer's recommendations (Invitrogen, Carlsbad, CA). Cultures were maintained at >90% viability on a shaker plate (Titer Plate Shaker; Lab-Line Instruments, Melrose Park, NJ) moving at 125 rpm in a 37°C incubator with 8% CO_2 and subculturing at a 1:10 ratio upon reaching a density of 2×10^6 cells per ml. Cell density and viability were evaluated with a hemocytometer using 0.4% trypan blue staining. After 96 h, the transfected cell culture was harvested. The supernatant containing the secreted recombinant protein was centrifuged (100×g, 15 min), frozen, and stored at −30°C until use. The 293-F cells supernatant containing the recombinant protein was loaded onto a Ni^{2+} column (Amersham Biosciences) following the manufacturer's directions. Fractions were eluted with 80, 100, 250, and 1000 mM imidazole (in 50 mM Tris, 300 mM NaCl, pH 8.0), and the fraction eluted at 250 mM was pooled and concentrated in an Amicon (10 kDa molecular weight cutoff) to 1 ml (Amersham Biosciences).

Western blot analyses

Purified recombinant protein was loaded onto 12% sodium dodecyl sulfate gels. Proteins were detected with goat anti-IL28 (1:2000) polyclonal antibody (Santa Cruz Biotechnology, Santa Cruz, CA) and the secondary antibody. Proteins were visualized using ECL Plus Western blotting detection reagents (GE Healthcare) and a LuminoImager (LAS-3000; Fujifilm). The band densities were analyzed with the Multi Gauge software (version 3.1; Fujifilm).

IL-28A/B promoter genotyping

Germ-line DNA was extracted from PBMC according to standard methods [14]. Twenty HV samples were genotyped for the dinucleotide insertion/deletion (indel) present in the promoter region of *IL-28A* or *B*, as described below. Twenty ng of genomic DNA were subjected to PCR analysis in 50 µl aliquots containing

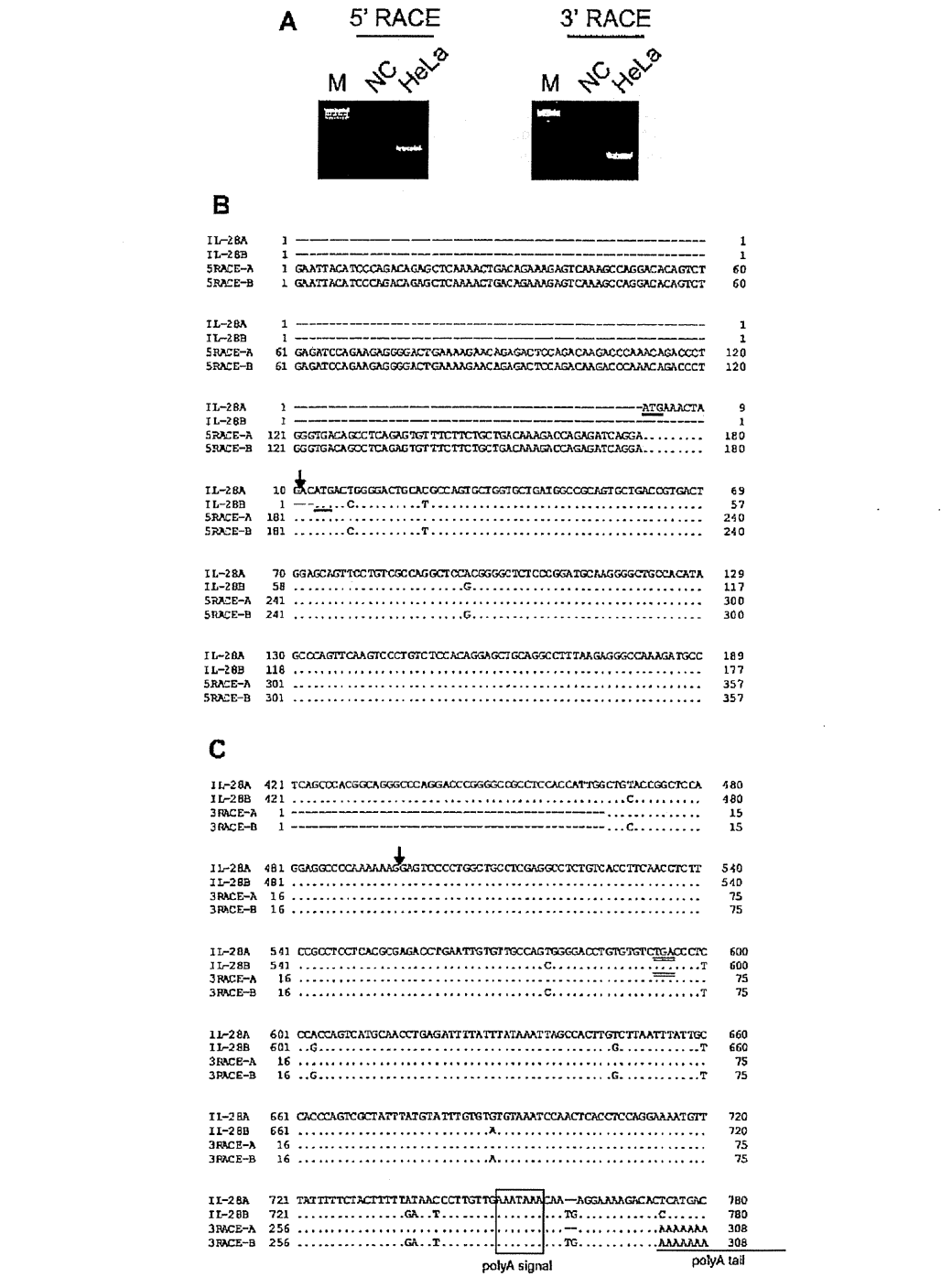
A
5' RACE
3' RACE
M
NC
HeLa
M
NC
HeLa
B
C
polyA signal
polyA tail
D
TSS
IL-28B
I
II
III
IV
V
VI
No.
1
2
3
4
5

Figure 2. The determination of IL-28B gene structure and UTR region. *IL-28A/B* cDNA was isolated using a complete cDNA cloning method and the entire sequences were determined using HeLa, MT-2, and Raji cell lines and PBMC from healthy volunteers. (A) 5′- and 3′-RACE analyses were used to determine the complete sequence of *IL-28A/B* mRNA after LPS stimulation (3 μg/mL) for 4 h following IFN-α treatment (100 U/mL) for 16 h. A representative example of agarose gel electrophoresis is shown for the non-stimulated control (NC). PCR products were inserted into the cloning vector and 6 clones of 5′- and 3′-RACE were analyzed by sequencing. (B) mRNA sequences of the 5′ terminal region were aligned using CCDS retrieved from NCBI and RACE data of *IL-28A/B*. The upper two sequences are reference sequences from the NCBI CCDS and the lower two are representative sequences of *IL-28A* and *28B* obtained from 5′-RACE. The underlined triplet indicates the start codon of each gene and arrow shows the splice junctions. (C) mRNA sequences of the 3′ terminal region were aligned using CCDS retrieved from NCBI and RACE data from *IL-28A/B*. The double-underlined triplet indicates the stop codon of each gene and arrows show the splice junctions. The polyA signal and representative site of polyadenylation also are shown. (D) The derived gene structure of the *IL-28B* is shown with the significant SNPs. The location of SNP No. 3 was changed from the regulatory to an intron region. The transcription start site (TSS) is found behind SNP No. 2.
doi:10.1371/journal.pone.0026620.g002

20 pmol of each primer, 5×PrimeSTAR GXL Buffer, 2.5 mM each deoxynucleotide triphosphates, and 1.25 units of PrimeStar GXL DNA polymerase (TAKARA Bio Inc, Tokyo, Japan). The primer pair, G1 and G2 (listed in Table S1), was used for the simultaneous amplification of the *IL-28A* and *28B* regulatory regions. The PCR conditions were as follows: 30 cycles of 10 s at 98°C, and 120 s at 68°C in addition of initial denaturation at 98°C for 5 min and a final extension at 68°C for 10 min. To separate the *IL-28A* amplicon from that of *IL-28B*, 10 μl of PCR products were analyzed using agarose gel electrophoresis and extracted with QIAquick Gel Extraction Kit (Qiagen). Each extracted product was analyzed by direct sequencing using Seq1 and Seq2 primers (Table S1). For further testing of the TA repeat, heterozygous samples were cloned into the pGEM-Teasy vector to count the number of TA repeats in each allele. Six clones were isolated and subjected to sequencing analysis using the primers described above.

Reporter assay

Luciferase assays of recombinant protein were performed using Dual-Glo Luciferase reporter assay system (Promega, Fitchburg, WI). In toll-like receptor (TLR)-stimulated experiments Raji cells were transfected and left for 16 h with 100 U/mL of IFN-α, then were exposed to LPS (3 μg/ml) for 4 h before harvesting. For assessments of recombinant protein, HeLa cells were transfected with pISRE-Luc and pGL4.74, and were harvested 24 h after IFN-α or λ treatment. The chemiluminescence was measured by SpectraMax L (Molecular Devices, Sunnyvale, CA). Firefly luciferase activity was normalized to Renilla activity to adjust for transfection efficiency.

Real-time PCR detection

Jurkat cells were transfected with the *IL-28B* expression vector harboring a FLAG sequence derived from the natural promoter (pdCMV/MA, mi, or AS). To induce IL-28B expression, TLR and IFN-α stimulation was given as described above. FLAG and glyceraldehyde-3-phosphate dehydrogenase (GAPDH) mRNA expression were measured using a real-time PCR performed on ABI Prism 7700 sequence detection system (Applied Biosystems) using primer sets (Table S1) after total RNA extraction and reverse transcription (RT) using an RT kit and TaqMan Universal PCR master mix (both Applied Biosystems), according to the manufacturer's manual. Relative gene expression was calculated as a fold induction compared to the control. Data were analyzed by the 2[-Delta Delta C(t)] method using Sequence Detector version 1.7 software (Applied Biosystems) [18] and were normalized using human GAPDH. A standard curve was prepared by serial 10-fold dilutions of human cDNA or FLAG plasmid. The curve was linear over 7 logs with a 0.998 correlation coefficient.

Statistical Analysis

Statistical analyses were conducted by using SPSS software package (SPSS 18J, SPSS, Chicago, IL) and Microsoft Excel 2007 (Microsoft co., Redmond, WA). Discrete variables were evaluated by Fisher's exact probability test. The P values were calculated by two-tailed student's t-tests for continuous data and chi-square test for categorical data, and those of less than 0.05 were considered as statistically significant.

Results

The identification of IL-28B gene structure

To define the human *IL-28A* or *IL-28B* gene structure, 5′-RACE and 3′-RACE were performed on total extracted RNA from HeLa, MT-2, Raji, HuH7 cells, and PBMCs from healthy volunteers (Fig. 2A). The sequences obtained matched the genomic contig of AC011445, which contains the sequence of *IL-28A* and *IL-28B* in forward and reverse orientations, respectively. All intron/exon junctions conformed to the canonical GT-AG rule. After stimulation of cells with LPS (3 μg/ml) for 4 h following IFN-α treatment (100 U/mL) for 16 h, *IL-28A/B* transcripts were detected in RACE experiments, but these were not detected in unstimulated cells. The representative TSSs are shown in Fig. 2B and showed little variation among cloned mRNA transcripts. The same 3′-UTR fragment also was detected without any intron in the 3′-RACE experiments (Fig. 2C). A polyadenylation signal (AAAUAAA), located in the 3′-UTR, was found upstream of the polyadenylation site in all samples. All sequences from the transcripts were aligned on the 5′-UTR, the six exons, and the 3′-UTR region of *IL-28A/B*. No different mRNA transcripts of *IL-28A/B* were found in our experiment. Taken together, the *IL-28B* gene structure comprised six exons (see Fig. 2D), and the location of SNP no. 3 (rs28416813) is in an intron, rather than a regulatory region (Table 1).

The effect of regulatory SNPs on promoter activity

Because the TSS was upstream of the position described in previous reports (Fig. 2), two rSNPs (rs72258881 and rs4803219) in the regulatory region were more specifically located in the TSS. A luciferase reporter approach was used to assess the effects of the two rSNPs on promoter activity. Luciferase vectors harboring the rSNPs were constructed and used for transfections (Fig. 3A). The promoter activities of the constructs were measured after stimulation with LPS (3 μg/ml) for 4 h following IFN-α treatment (100 U/mL) for 16 h. The transcriptional activity of constructions harboring the $(TA)_{11}$ mutation was reduced (Fig. 3B). Substitution in the rSNP (rs4803219) showed little effect on the transcriptional activity, whereas the number of TA repeats could be responsible for the putative region controlling basal transcription. To confirm the transcriptional activity, Jurkat cells were transfected with full length constructs expressing the FLAG sequence under the control of the natural promoter (Fig. 3C). To avoid the detection of endogenous mRNA, the mRNA with the FLAG sequence was specifically detected by real time PCR using the FLAG primer. The constructs harboring $(TA)_{11}$ yielded lower expression levels

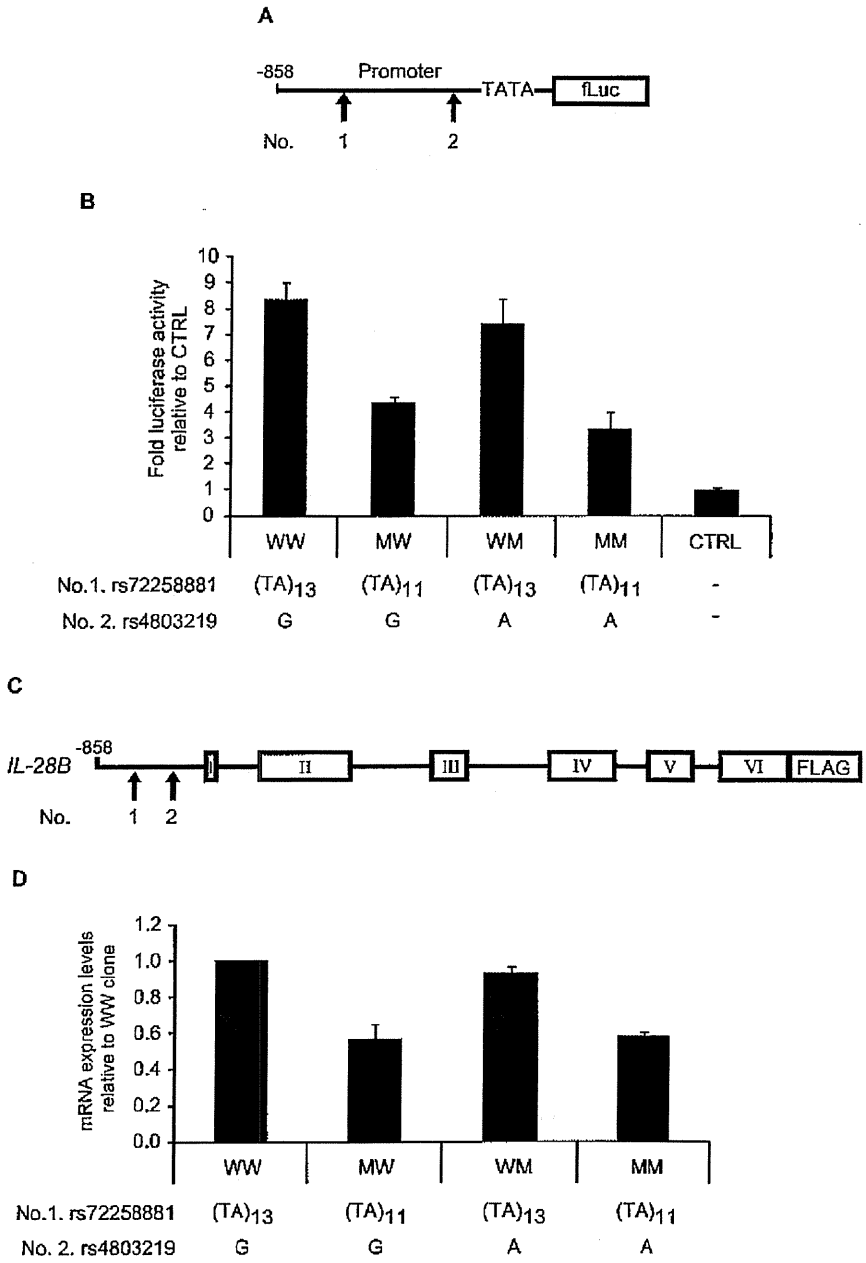

Figure 3. Transcriptional activity of the IL-28B promoter region compared between major and minor alleles. (A) The pGL4 reporter plasmid was constructed by subcloning the *IL-28B* promoter subfragment (nt −858 to +30). The combinations of two regulatory SNPs (rs72258881 or rs4803219) were introduced into the pGL4 vector (pGL4/WW, MW, WM, and MM). (B) Raji cells were co-transfected with pGL4 plasmids (0.05 g), and pGL4.74 control plasmid (0.05 g), and tested for firefly as well as renilla luciferase after LPS stimulation (3 μg/mL) for 4 h following IFN-α treatment (100 U/mL) for 16 h. These cells were seeded in a 96-well plate at 10^4 cells/well. The luciferase activities were normalized with renilla activities and data are presented as fold induction from activation of control vector. Bars indicate the means ± SD of triplicate determinations and the results are from one of three experiments. Statistical analyses are shown in table S2 to avoid complication. (C) For real-time PCR, the combinations of two regulatory SNPs (rs72258881 or rs4803219) were introduced into the pdCMV vector harboring a FLAG sequence (pdCMV/WW, MW, WM, and MM). (D) Jurkat cells were co-transfected with pdCMV plasmids (0.05 μg) and secreted alkaline phosphatase (SEAP) control plasmid (0.05 μg) and the expression levels were quantified using specific primer after LPS and IFN-α stimulation. The FLAG expression levels were normalized with SEAP activities and GAPDH as described in method section. Data are presented as fold induction from expression levels of pdCMV/WW. Bars indicate the means ± SD of triplicate determinations and the results are from one of three experiments. Statistical analyses are shown in table S3 to avoid complication.

doi:10.1371/journal.pone.0026620.g003

after IFN-α and LPS stimulation (Fig. 3D), suggesting that the length of TA repeat in the regulatory region of *IL-28B* could affect the regulation of *IL-28B* transcription.

Two intron SNPs located near the branch site of splicing

To determine the effect of the two iSNPs on pre-mRNA splicing, HeLa cells were transfected with wild type (WT), a construct with a double mutation of the iSNPs (d-iSNPs), or an antisense (AS) plasmid driven by the CMV promoter (Fig. 4A). The construct providing antisense transcription controlled by the CMV promoter was used to control for splicing defects (AS). Transcripts were analyzed by RT-PCR using primers in exon 1–2, 3–4, and 4–5. The RNA isolated from the WT and d-iSNPs yielded a single band using the three primer pairs. In contrast, longer amplicons were generated in cells expressing the antisense construct (Fig. 4B). The PCR products were sequenced to confirm the origin of the aberrant splicing events derived from the antisense construct (data not shown). The sequence analyses confirmed that PCR products from the WT and d-iSNPs were generated by normal splicing, suggesting that these two intron SNPs resulted in no splicing defects under these conditions.

No effect of nonsynonymous SNPs on IL-28B function

A nonsynonymous SNPs (rs8103142) located in the 3rd exon (Table 1 and Fig. 2D) led to the amino acid substitution $K^{74}R$ (Fig. 5A). Interestingly, the amino acid at this position is almost always arginine in homologous mammalian IFN-λs (e.g. human IL-28A, mouse IL-28A/B, and rhesus IL-28A/B). Then, the $K^{74}R$ substitution was expected to change IL-28B activity. The purified recombinant IL-28B protein (wild type) and the variant (ns-mut) were recognized by anti-IL-28B polyclonal antibody in a western blot assay (Fig. 5B). Based on spectrophotometric measurement of the protein concentration of the eluted fraction, it was calculated that at least 360 μg/mL of purified recombinant IL-28B protein (wild type and ns-mut) was obtained after purification. Flow-through liquid without recombinant protein was provided in the column preparing the sample of pcDNA3.1/AS (Fig. 5B). Molecular processing of IL-28B protein was confirmed to determine the precise N-terminal amino acid by peptide sequencer as the processing site of signal peptide was predicted by computer simulation (http://www.uniprot.org/uniprot/Q8IZI9). Then, the N-terminal sequence, VPVAR, was obtained (data not shown), suggesting that the simulation data was consistent with the form of physiological protein.

To evaluate the effect of nsSNPs on ISRE activity, three hepatoma cell lines (HuH7, HepG2, and HuSE2) expressing IL-28R1 and IL-10R2 were transfected with pISRE-Luc and pGL4.74. These recombinant proteins were added to the supernatant (5 ng/mL each). As shown in Fig. 5C, ISRE activity of the ns-mut protein was similar to that of wild type protein in each cell line. IFN-α (100 U/mL), as a positive control of ISRE activity, showed a strong ISRE activity. These results suggested that the nonsynonymous mutation of rs8103142 did not affect IL-28B activity *in vitro*.

The genetic variation of TA repeats at the upstream of *IL-28B*

The reference sequence (RefSeq) of the human genome in the international database registers the TA repeat SNPs, rs72284729 or rs72258881, in the regulatory regions of *IL-28A* and *IL-28B*, respectively. The registered basal number of $(TA)_n$ is 8 in the regulatory region of *IL-28A* on the plus strand, whereas that of *IL-28B* is 13 on the minus strand encoding the gene (Table 2). From 20 Japanese healthy volunteers, genomic DNA was extracted to determine the actual $(TA)_n$ number located in the region of *IL-28A* or *IL-28B* by direct sequencing and, when direct sequencing chromatographs of $(TA)_n$ heterozygotes showed mixed patterns from the end of the TA repeat (Fig. S4), the mixed samples were subjected to cloning analysis. Interestingly, the $(TA)_n$ number in *IL-28A* was consistently different from dbSNP data, whereas that of *IL-28B* showed varying numbers along with SNPs data. The $(TA)_n$ range of *IL-28B* was from 10 to 18, and the most prevalent genotype was 12/12 (75%) in healthy Japanese volunteers.

To determine the functional significance of the TA indel, the regulatory region from −858 bp to +30 bp modifying the $(TA)_n$ number was cloned into the pGL4 reporter vector, transfected into HeLa cells, and assessed for firefly luciferase reporter gene

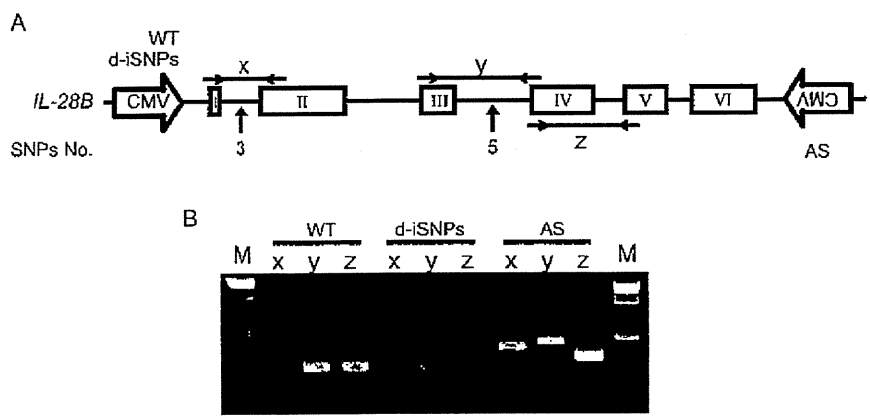

Figure 4. The determination of intron SNPs located near the branch site of splicing. (A) The expression plasmid of WT, d-iSNPs, or antisense (AS) derived from the CMV promoter was transfected into HeLa cells. Schematic of the WT, d-iSNPs, or AS used in the transfection experiments. PCR primers were designed to amplify products between exons. The effect of No. 3 and 5 SNPs (rs28416813 or rs11881222) on splicing were examined by amplicons x and y, respectively. The amplicon z was used for a splicing control. (B) Isolated RNAs were amplified by RT-PCR. The amplified products were checked by 2% agarose gel electrophoresis. The bands from the AS plasmid transcribing antisense represented abnormal splicing of mRNA as a control. Results shown are representative of three independent experiments.
doi:10.1371/journal.pone.0026620.g004

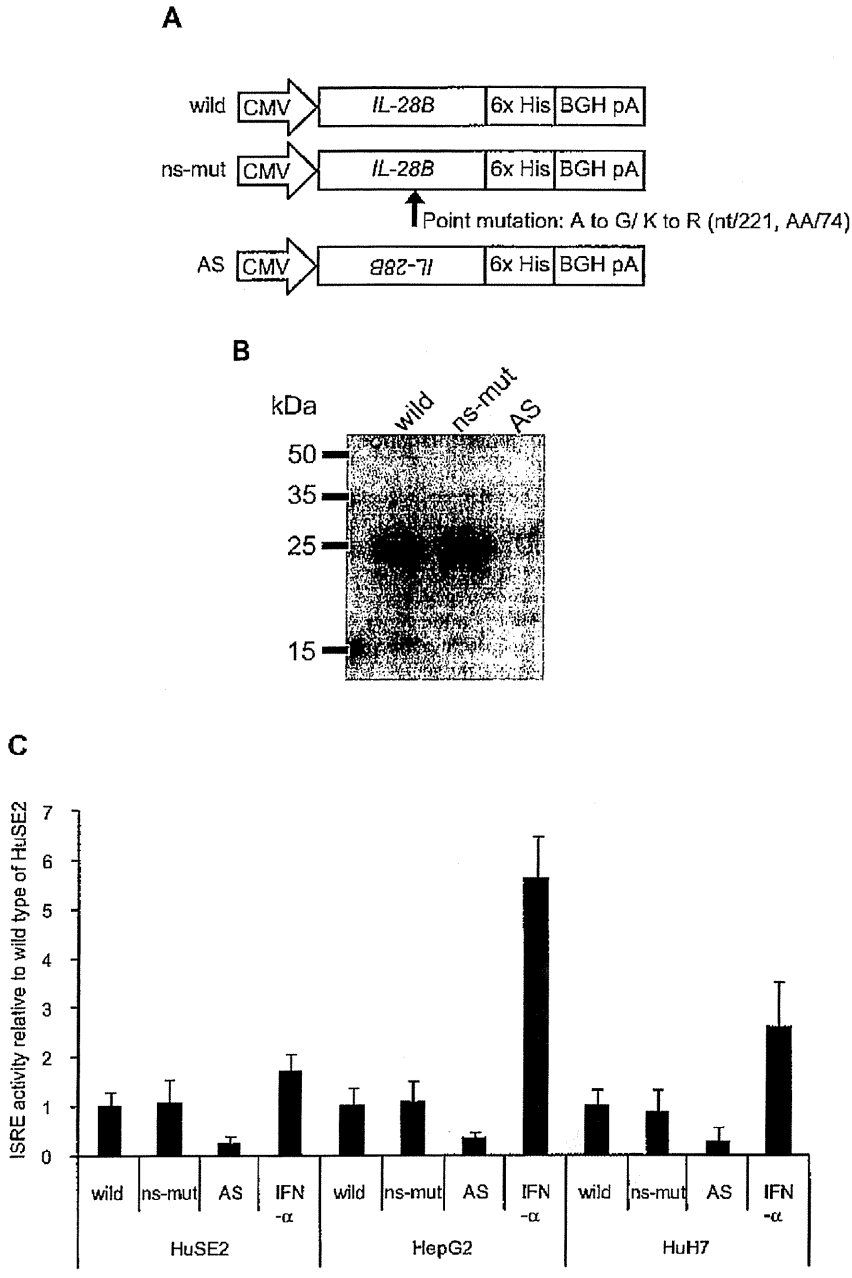

Figure 5. The purification and the activity of recombinant IL-28B with or without nsSNP. (A) The 6×His-tagged expression plasmid of wild type, ns-mut, or AS controlled by the CMV promoter was transfected into 293F cells. Schematics are the wild type, ns-mut and AS used in the transfection experiments. The procedure for recombinant protein purification is described in the materials and methods section. (B) The purified products were confirmed by immunoblotting using anti-IL28B antibody and the secondary antibody. The prepared proteins were loaded onto a 12% polyacrylamide gel. Bands corresponding to the expected molecular weight of IL-28B were observed in the wild type and ns-mut lanes. (C) For luciferase assay, HeLa cells were seeded into a 96-well plate at 10^4 cells/well and transfected with pISRE-Luc and pGL4.74 control vector before 16 h of IFN-α or IL-28B stimulation. Five ng/mL of IL-28B wild or ns-mut was added to the culture medium. Flow-though liquid from AS expression was used as a negative control. IFN-α (100 U/mL) was added for positive control of ISRE activity. The luciferase activities were normalized with Renilla activities and data are presented as fold induction from the basal promoter activation of the wild type. Bars indicate the means ± SD of triplicate determinations and the results are from one of three experiments.
doi:10.1371/journal.pone.0026620.g005

Table 2. The variations of TA repeat in *IL-28A* and *28B*.

		Location	
Gene	Data	rs72284792*[1]	rs72258881
IL-28A	RefSeq. (hg19)	$(TA)_6$	
	Cloning	$(TA)_6$	
IL-28B	RefSeq. (hg19)		$(TA)_{13}$
	Cloning		$(TA)_{10-18}$

*[1]The ID represents rs72258881, rs59702201, and rs67461793 because these three are located in the same genomic region, the TA repeat.
doi:10.1371/journal.pone.0026620.t002

expression (Fig. 6A). These cells were treated with 100 U/mL of IFN-α and 3 μg/mL of LPS. The results indicated that the variation in the $(TA)_n$ number at this polymorphic locus differentially regulates transcription. The transcriptional activation of the luciferase reporter gene was increased according to the $(TA)_n$ number (Fig. 6B).

Discussion

Four independent GWAS approaches have revealed the significant SNPs associated with response to PEG-IFNα/RBV therapy for CHC [12,13,14,19]. These significant SNPs were found around *IL-28B* but not *IL-28A*. The SNPs found in clinical studies to determine the outcome of HCV therapy were rs12979860 and rs8099917, because they showed the statistical significance in each study [12,13,14,19]. However, several SNPs around *IL-28B* were in strong LD (r^2>0.96) in JPT and CEU populations, although relatively low LD was predicted in the YRI population [16], and so it might be difficult to determine the most informative SNP [16]. These results suggest that any of the SNPs contained in this region could be of predictive value.

As reported in previous studies, transcription of *IL-28A/B* was upregulated in the TT genotype of rs8099917, which was associated with SVR [13,14,20], suggesting that the expression levels of *IL-28B* could be one of the key factors to clear HCV under PEG-IFNα/RBV therapy and could also affect spontaneous clearance of acute HCV infection [15]. To elucidate this question, we examined the function of the SNPs around the *IL-28B* gene to identify those SNPs affecting *IL-28B* expression. The new findings are as follows: 1) the gene structure of *IL-28B* comprised six exons in the several cell lines tested, although it was registered as having five exons in the CCDS database of NCBI. 2) The substitution of intron SNPs and non-synonymous SNPs in the *IL-28B* gene did not influence the expression levels or function. 3) Increased numbers of TA repeats in the promoter region of the *IL-28B* gene enhanced the transcription activity and expression level of the *IL-28B* gene. Because administration of IL-28B has been shown to have antiviral effects [21,22,23], lower expression of IL-28B might lead to a decrease in this effect.

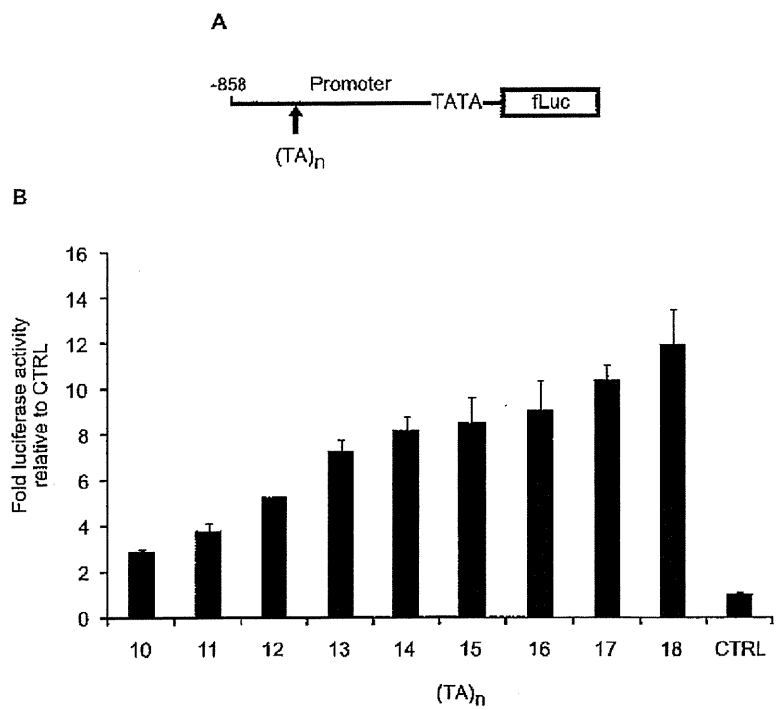

Figure 6. Luciferase assay of $(TA)_n$ number. (A) *IL-28B* promoter subfragment (nt −858 to +30) modifying $(TA)_n$ number from 10 to 18 was constructed in the pGL4 vector. (B) Raji cells were co-transfected with pGL4 plasmids (0.05 g), and pGL4.74 control plasmid (0.05 g), and tested for firefly as well as renilla luciferase after LPS stimulation (3 μg/mL) for 4 h following IFN-α treatment (100 U/mL) for 16 h. These cells were seeded into a 96-well plate at 10^4 cells/well. The luc activities were normalized with renilla activities and data are presented as fold induction from the activation of the control vector. Bars, the means ± SD of triplicate determinations and the results are from one of three experiments. Statistical analyses are shown in table S4 to avoid complication.
doi:10.1371/journal.pone.0026620.g006

The locations of two SNPs associated with response to HCV therapy, rs8099917 and rs12979860, are approximately 8 kb and 3 kb upstream of *IL-28B* gene, respectively. Because these SNPs, which showed the greatest statistical significance in the previous study, are located far from the *IL-28B* gene, another approach was required to determine the effect of the SNPs. In this study, broad $(TA)_n$ variations were observed in rs8099917 heterozygotes among CHC patients. Interestingly, a combination of TG and 11/12 genotype was strongly associated with NVR, whereas patients harboring the 12/13 genotype showed a virological response, regardless of the TG genotype (rs8099917). In clinical practice, genetic diagnosis using TA variation, following the primary classification of rs8099917 genotype, could improve the prediction of treatment response for CHC patients with the rs8099917 TG genotype. It is not clear whether the variation originates from genetic or epigenetic mechanisms. In addition, as the frequency of TA variation might be dependent on the particular population, further study will be needed to compare the frequency in several populations. A long TA repeat, over $(TA)_{13}$, was observed in healthy volunteers and showed potential for higher gene expression compared with under $(TA)_{13}$ constructs *in vitro*. It may be possible that spontaneous clearance of HCV infection and CHC patients are affected by this region because this also is dependent on *IL-28B* genotype [15,19]. In our speculation, the combination of both TA variation and the landmark SNPs, rs8099917 and rs12979860, might improve the prediction value. In addition, convenient diagnosis method to detect the TA variation like SNPs typing is needed since the present capillary techniques are relative complexity compared with SNPs typing.

In the international database, some SNPs ID are registered in the TA repeat region, located in the regulatory regions of the *IL-28A* and *IL-28B* gene, rs72284792 and rs7225881, respectively, whereas in our analysis separating *IL-28A* from *IL-28*, TA variation was detected only in the *IL-28B* region. SNP data often have been collected using next generation sequencing and based on short sequence reads. Unfortunately, the sequence similarity between *IL-28A* and *IL-28B* is over 90% from the CpG island to the region downstream of 3′-UTR. Alignment failure would occur for a high percentage of sequences when analyzed with software using general algorithms.

Effects of insertion/deletion (indel) polymorphism are known in the field of pharmacogenetic research. A polymorphism in the promoter of the uridine diphosphoglucuronosyl transferase 1A1 (*UGT 1A1*) gene has been shown to cause Crigler-Najjar syndrome types I and II and Gilbert syndrome, a benign form of unconjugated hyperbilirubinemia, and the occurrence of severe toxic events in irinotecan (known as CPT-11) administration [24,25,26]. The polymorphism consists of a $(TA)_n$ repeat in the 5′-promoter region [24,26,27], similar to that in this study. The range of repeat numbers is from $(TA)_5$ to $(TA)_8$ in the *UGT 1A1* gene [28]. The genetic disorder of the TA repeat length affects enzyme activity. The hepatic bilirubin *UGT1A1* activity of individuals with Gilbert's syndrome is <30% of normal [29]. Irinotecan is used or under evaluation for a broad spectrum of solid tumors. Irinotecan pharmacokinetic parameters display a wide inter-patient variability and are involved in the genesis of toxic side effects [30,31,32,33]. Based on the polymorphism of the TA repeat, previous papers reported the association of irinotecan-induced severe toxicity with Gilbert's syndrome [34,35,36]. The value of genetic diagnosis of the *UGT1A1* polymorphisms prior to irinotecan chemotherapy has been corroborated in a previous study [37]. As similar characteristics were observed in the upstream region of *IL-28B*, the $(TA)_n$ repeat might be associated with disease progression as well as response to anti-HCV treatment.

In terms of epigenetic aspects, the TA variation of *IL-28B* was also suspected to be related to microsatellite instability, because a gap between the significant SNPs and TA variation was observed in this study. DNA mismatch repair (MMR) deficiency causes a high frequency of microsatellite instability (MSI-H), which is characterized by length alterations within simple repeated sequences, microsatellites. Lynch syndrome is primarily due to germline mutations in one of the DNA MMR genes, hMLH1 or hMSH2 [38]. MSI-H is also observed in <15% of colorectal, gastric and endometrial cancers, where it is associated with the hypermethylation of the promoter region of hMLH1 [39,40]. The diagnosis of MSI-H in cancers is therefore useful for identifying patients with Lynch syndrome and the efficacy of chemotherapy [41,42,43,44,45,46].

In conclusion, a (TA) dinucleotide repeat, rs72258881, located in the promoter region, was discovered by our functional studies of the proximal SNPs around *IL-28B*; the transcriptional activity of the promoter increased gradually in a $(TA)_n$ length-dependent manner. Combination diagnosis based on rs8099917 and rs72258881 might provide improved prediction because the $(TA)_n$ variation of *IL-28B* was observed but not that of *IL-28A*. The further study is needed to reveal the association with treatment response using clinical specimens of CHC. These findings suggest that the dinucleotide repeat could be associated with the transcriptional activity of *IL-28B* as well as constituting a predictor to improve prediction of the response to interferon-based HCV treatment.

Supporting Information

Figure S1 Sequence alignment of *IL-28A/B* cDNA retrieved from the database. The cDNA sequences of *IL-28A/B* were retrieved from the international database using accession number. The cDNA data reported by Sheppard et al. are AY129148 (*IL-28A*) and AY129149 (*IL-28B*) indicated with '_S' in the figure, and that of Kotenko et al. are AY184373 (*IL-28A*) and AY184374 (*IL-28B*) indicated with '_K'. Dashed boxes show the start codon predicted by computational analysis of the human genome reported by Sheppard et al. and Kotenko et al. The sequence alignment was calculated with Lasergene software (DNASTAR, Madison, WI).
(PDF)

Figure S2 Structural similarity between *IL-28A* and *IL-28B*. (A) Schematic of *IL-28A/B* gene location (UCSC genome browser). Boxes show the region representing high levels of structural similarity around *IL-28A/B*. (B) Modified schematic of structural similarity with a percentage. (C) Alignment between IL-28A and IL-28B from the CpG island to the region downstream of 3′-UTR. Homologous regions are shown by red characters. High levels of structural similarity were observed in CpG island, regulatory and gene region bypassing the in/del site.
(PDF)

Figure S3 Innate immune receptor expression related to IL-28B regulation. The relevant receptors for this study were confirmed by PCR using specific primers. (A) The mRNA expression of TLR4 was detected in cell lines, HeLa, Jurkat, MT-2, Raji, and PBMC. (B) For the study of cytokine-receptor association, the expression of IL-28RA and IL-10RB second receptor were examined using cDNA obtained from HuH7, HepG2, and HuSE2 cells. Samples without reverse transcriptase were prepared as a negative control in addition to the checking of genome contamination.
(PDF)

Figure S4 Direct sequencing analysis of TA repeat. In the first step to determine $(TA)_n$ genotypes, direct sequencing was

applied to amplicons of *IL-28A* or *28B* separated by gel electrophoresis. Homozygotes of TA repeat showed clear patterns and a high quality value in the bar above, whereas the patterns of heterozygotes were mixed because the length differed between alleles. The mixed patterns are shown in dashed boxes. These mixed products were cloned into the pGEM-Teasy vector to isolate and count the $(TA)_n$ number by sequencing of both alleles. (PDF)

Table S1
(DOC)

Table S2
(DOC)

Table S3
(DOC)

Table S4
(DOC)

Acknowledgments

We gratefully acknowledge Dr. Naoya Sakamoto for help with reporter vector (Tokyo Medical and Dental University). We also thank the following for their technical assistance: Dr. Shuko Murakami, Ms. Hatsue Naganuma, Ms. Kyoko Akita (Nagoya City University).

Author Contributions

Conceived and designed the experiments: MS YT MN TW MM. Performed the experiments: MS YT. Analyzed the data: MS YT. Contributed reagents/materials/analysis tools: MS YT MN TW MM. Wrote the paper: MS YT MN TW MM.

References

1. Kotenko SV, Gallagher G, Baurin VV, Lewis-Antes A, Shen M, et al. (2003) IFN-lambdas mediate antiviral protection through a distinct class II cytokine receptor complex. Nat Immunol 4: 69–77.
2. Sheppard P, Kindsvogel W, Xu W, Henderson K, Schlutsmeyer S, et al. (2003) IL-28, IL-29 and their class II cytokine receptor IL-28R. Nat Immunol 4: 63–68.
3. Mordstein M, Kochs G, Dumoutier L, Renauld JC, Paludan SR, et al. (2008) Interferon-lambda contributes to innate immunity of mice against influenza A virus but not against hepatotropic viruses. PLoS Pathog 4: e1000151.
4. Sommereyns C, Paul S, Staeheli P, Michiels T (2008) IFN-lambda (IFN-lambda) is expressed in a tissue-dependent fashion and primarily acts on epithelial cells in vivo. PLoS Pathog 4: e1000017.
5. Doyle SE, Schreckhise H, Khuu-Duong K, Henderson K, Rosler R, et al. (2006) Interleukin-29 uses a type 1 interferon-like program to promote antiviral responses in human hepatocytes. Hepatology 44: 896–906.
6. Marcello T, Grakoui A, Barba-Spaeth G, Machlin ES, Kotenko SV, et al. (2006) Interferons alpha and lambda inhibit hepatitis C virus replication with distinct signal transduction and gene regulation kinetics. Gastroenterology 131: 1887–1898.
7. Zhou Z, Hamming OJ, Ank N, Paludan SR, Nielsen AL, et al. (2007) Type III interferon (IFN) induces a type I IFN-like response in a restricted subset of cells through signaling pathways involving both the Jak-STAT pathway and the mitogen-activated protein kinases. J Virol 81: 7749–7758.
8. Bartlett NW, Buttigieg K, Kotenko SV, Smith GL (2005) Murine interferon lambdas (type III interferons) exhibit potent antiviral activity in vivo in a poxvirus infection model. J Gen Virol 86: 1589–1596.
9. Brand S, Zitzmann K, Dambacher J, Beigel F, Olszak T, et al. (2005) SOCS-1 inhibits expression of the antiviral proteins 2',5'-OAS and MxA induced by the novel interferon-lambdas IL-28A and IL-29. Biochem Biophys Res Commun 331: 543–548.
10. Robek MD, Boyd BS, Chisari FV (2005) Lambda interferon inhibits hepatitis B and C virus replication. J Virol 79: 3851–3854.
11. Zhu H, Butera M, Nelson DR, Liu C (2005) Novel type I interferon IL-28A suppresses hepatitis C viral RNA replication. Virol J 2: 80.
12. Ge D, Fellay J, Thompson AJ, Simon JS, Shianna KV, et al. (2009) Genetic variation in IL28B predicts hepatitis C treatment-induced viral clearance. Nature 461: 399–401.
13. Suppiah V, Moldovan M, Ahlenstiel G, Berg T, Weltman M, et al. (2009) IL28B is associated with response to chronic hepatitis C interferon-alpha and ribavirin therapy. Nat Genet 41: 1100–1104.
14. Tanaka Y, Nishida N, Sugiyama M, Kurosaki M, Matsuura K, et al. (2009) Genome-wide association of IL28B with response to pegylated interferon-alpha and ribavirin therapy for chronic hepatitis C. Nat Genet 41: 1105–1109.
15. Thomas DL, Thio CL, Martin MP, Qi Y, Ge D, et al. (2009) Genetic variation in IL28B and spontaneous clearance of hepatitis C virus. Nature 461: 798–801.
16. Tanaka Y, Nishida N, Sugiyama M, Tokunaga K, Mizokami M (2010) lambda-Interferons and the single nucleotide polymorphisms: A milestone to tailor-made therapy for chronic hepatitis C. Hepatol Res 40: 449–460.
17. Siren J, Pirhonen J, Julkunen I, Matikainen S (2005) IFN-alpha regulates TLR-dependent gene expression of IFN-alpha, IFN-beta, IL-28, and IL-29. J Immunol 174: 1932–1937.
18. Livak KJ, Schmittgen TD (2001) Analysis of relative gene expression data using real-time quantitative PCR and the 2(-Delta Delta C(T)) Method. Methods 25: 402–408.
19. Rauch A, Kutalik Z, Descombes P, Cai T, Di Iulio J, et al. (2010) Genetic variation in IL28B is associated with chronic hepatitis C and treatment failure: a genome-wide association study. Gastroenterology. pp 138–1338–1345, 1345 e1331–1337.
20. Fukuhara T, Takctomi A, Motomura T, Okano S, Ninomiya A, et al. (2010) Variants in IL28B in liver recipients and donors correlate with response to peg-interferon and ribavirin therapy for recurrent hepatitis C. Gastroenterology. pp 139–1577–1585, 1585 e1571–1573.
21. Ank N, Iversen MB, Bartholdy C, Staeheli P, Hartmann R, et al. (2008) An important role for type III interferon (IFN-lambda/IL-28) in TLR-induced antiviral activity. J Immunol 180: 2474–2485.
22. Ank N, West H, Bartholdy C, Eriksson K, Thomsen AR, et al. (2006) Lambda interferon (IFN-lambda), a type III IFN, is induced by viruses and IFNs and displays potent antiviral activity against select virus infections in vivo. J Virol 80: 4501–4509.
23. Contoli M, Message SD, Laza-Stanca V, Edwards MR, Wark PA, et al. (2006) Role of deficient type III interferon-lambda production in asthma exacerbations. Nat Med 12: 1023–1026.
24. Bosma PJ, Chowdhury JR, Bakker C, Gantla S, de Boer A, et al. (1995) The genetic basis of the reduced expression of bilirubin UDP-glucuronosyltransferase 1 in Gilbert's syndrome. N Engl J Med 333: 1171–1175.
25. Monaghan G, Ryan M, Seddon R, Hume R, Burchell B (1996) Genetic variation in bilirubin UPD-glucuronosyltransferase gene promoter and Gilbert's syndrome. Lancet 347: 578–581.
26. Raijmakers MT, Jansen PL, Steegers EA, Peters WH (2000) Association of human liver bilirubin UDP-glucuronyltransferase activity with a polymorphism in the promoter region of the UGT1A1 gene. J Hepatol 33: 348–351.
27. Sato H, Adachi Y, Koiwai O (1996) The genetic basis of Gilbert's syndrome. Lancet 347: 557–558.
28. Beutler E, Gelbart T, Demina A (1998) Racial variability in the UDP-glucuronosyltransferase 1 (UGT1A1) promoter: a balanced polymorphism for regulation of bilirubin metabolism? Proc Natl Acad Sci U S A 95: 8170–8174.
29. Yamamoto K, Sato H, Fujiyama Y, Doida Y, Bamba T (1998) Contribution of two missense mutations (G71R and Y486D) of the bilirubin UDP glycosyltransferase (UGT1A1) gene to phenotypes of Gilbert's syndrome and Crigler-Najjar syndrome type II. Biochim Biophys Acta 1406: 267–273.
30. Gupta E, Lestingi TM, Mick R, Ramirez J, Vokes EE, et al. (1994) Metabolic fate of irinotecan in humans: correlation of glucuronidation with diarrhea. Cancer Res 54: 3723–3725.
31. Gupta E, Mick R, Ramirez J, Wang X, Lestingi TM, et al. (1997) Pharmacokinetic and pharmacodynamic evaluation of the topoisomerase inhibitor irinotecan in cancer patients. J Clin Oncol 15: 1502–1510.
32. Rowinsky EK, Grochow LB, Ettinger DS, Sartorius SE, Lubejko BG, et al. (1994) Phase I and pharmacological study of the novel topoisomerase I inhibitor 7-ethyl-10-[4-(1-piperidino)-1-piperidino]carbonyloxycamptothecin (CPT-11) administered as a ninety-minute infusion every 3 weeks. Cancer Res 54: 427–436.
33. Iyer L, King CD, Whitington PF, Green MD, Roy SK, et al. (1998) Genetic predisposition to the metabolism of irinotecan (CPT-11). Role of uridine diphosphate glucuronosyltransferase isoform 1A1 in the glucuronidation of its active metabolite (SN-38) in human liver microsomes. J Clin Invest 101: 847–854.
34. Sugatani J, Yamakawa K, Yoshinari K, Machida T, Takagi H, et al. (2002) Identification of a defect in the UGT1A1 gene promoter and its association with hyperbilirubinemia. Biochem Biophys Res Commun 292: 492–497.
35. Iyanagi T, Emi Y, Ikushiro S (1998) Biochemical and molecular aspects of genetic disorders of bilirubin metabolism. Biochim Biophys Acta 1407: 173–184.
36. Wasserman E, Myara A, Lokiec F, Goldwasser F, Trivin F, et al. (1997) Severe CPT-11 toxicity in patients with Gilbert's syndrome: two case reports. Ann Oncol 8: 1049–1051.
37. Sadee W, Dai Z (2005) Pharmacogenetics/genomics and personalized medicine. Hum Mol Genet 14 Spec No. 2: R207–214.
38. Modrich P (1994) Mismatch repair, genetic stability, and cancer. Science 266: 1959–1960.
39. Lengauer C, Kinzler KW, Vogelstein B (1997) DNA methylation and genetic instability in colorectal cancer cells. Proc Natl Acad Sci U S A 94: 2545–2550.

40. Lengauer C, Kinzler KW, Vogelstein B (1997) Genetic instability in colorectal cancers. Nature 386: 623–627.
41. Kim GP, Colangelo LH, Paik S, O'Connell MJ, Kirsch IR, et al. (2007) Predictive value of microsatellite instability-high remains controversial. J Clin Oncol 25: 4857; author reply 4857–4858.
42. Elsaleh H, Joseph D, Grieu F, Zeps N, Spry N, et al. (2000) Association of tumour site and sex with survival benefit from adjuvant chemotherapy in colorectal cancer. Lancet 355: 1745–1750.
43. Gryfe R, Kim H, Hsieh ET, Aronson MD, Holowaty EJ, et al. (2000) Tumor microsatellite instability and clinical outcome in young patients with colorectal cancer. N Engl J Med 342: 69–77.
44. Ribic CM, Sargent DJ, Moore MJ, Thibodeau SN, French AJ, et al. (2003) Tumor microsatellite-instability status as a predictor of benefit from fluorouracil-based adjuvant chemotherapy for colon cancer. N Engl J Med 349: 247–257.
45. Popat S, Hubner R, Houlston RS (2005) Systematic review of microsatellite instability and colorectal cancer prognosis. J Clin Oncol 23: 609–618.
46. Sinicrope FA, Rego RL, Halling KC, Foster N, Sargent DJ, et al. (2006) Prognostic impact of microsatellite instability and DNA ploidy in human colon carcinoma patients. Gastroenterology 131: 729–737.

Hepatology Research

Hepatology Research 2011; 41: 936–945 doi: 10.1111/j.1872-034X.2011.00859.x

Original Article

Easy-to-use phylogenetic analysis system for hepatitis B virus infection

Masaya Sugiyama,[1,2]* Ayano Inui,[3] Tadasu Shin-I,[1] Haruki Komatsu,[3] Motokazu Mukaide,[1,4] Naohiko Masaki,[1] Kazumoto Murata,[1] Kiyoaki Ito,[1] Makoto Nakanishi,[2] Tomoo Fujisawa[3] and Masashi Mizokami[1]

[1]*The Research Center for Hepatitis and Immunology, National Center for Global Health and Medicine, Ichikawa,* [2]*Department of Biochemistry and Cell Biology, Nagoya City University Graduate School of Medical Sciences, Nagoya,* [3]*Department of Pediatrics, Eastern Yokohama Hospital, Yokohama, and* [4]*SRL, Inc. Tokyo, Japan*

Aim: The molecular phylogenetic analysis has been broadly applied to clinical and virological study. However, the appropriate settings and application of calculation parameters are difficult for non-specialists of molecular genetics. In the present study, the phylogenetic analysis tool was developed for the easy determination of genotypes and transmission route.

Methods: A total of 23 patients of 10 families infected with hepatitis B virus (HBV) were enrolled and expected to undergo intrafamilial transmission. The extracted HBV DNA were amplified and sequenced in a region of the S gene.

Results: The software to automatically classify query sequence was constructed and installed on the Hepatitis Virus Database (HVDB). Reference sequences were retrieved from HVDB, which contained major genotypes from A to H. Multiple-alignments using CLUSTAL W were performed before the genetic distance matrix was calculated with the six-parameter method. The phylogenetic tree was output by the neighbor-joining method. User interface using WWW-browser was also developed for intuitive control. This system was named as the easy-to-use phylogenetic analysis system (E-PAS). Twenty-three sera of 10 families were analyzed to evaluate E-PAS. The queries obtained from nine families were genotype C and were located in one cluster per family. However, one patient of a family was classified into the cluster different from her family, suggesting that E-PAS detected the sample distinct from that of her family on the transmission route.

Conclusions: The E-PAS to output phylogenetic tree was developed since requisite material was sequence data only. E-PAS could expand to determine HBV genotypes as well as transmission routes.

Key words: database, genotype, hepatitis B virus, intrafamilial transmission, phylogenetic analysis

INTRODUCTION

HEPATITIS B VIRUS (HBV) infects approximately 350 million people worldwide. Chronic HBV infection causes liver cirrhosis and liver cancer. In Japan, chronic hepatitis B patients are estimated to be approximately one million.[1] As HBV has high infectivity, almost all advanced countries have launched the universal infant immunization program against HBV. The patients with HB antigen seropositive, fulminant hepatitis and HCC have substantially declined in these countries.[2,3] The current immunization strategy represents favorable effects to prevent the HBV transmission. In countries without the universal vaccination program, however, substantial intrafamilial transmission and horizontal transmission have been reported.[4] In Japan, only high-risk infants born to chronic HBV-infected mothers have been given the HBV vaccine according to a selective vaccination policy of Japanese governments since 1986. This strategy has led to successful reduction of HBV carrier infants[5] since the major route of transmission has been perinatal transmission,[6,7] and horizontal transmission in early childhood has occurred as a result of close family contact.[8–10] However, the main

Correspondence: Dr Masashi Mizokami, The Research Center for Hepatitis and Immunology, National Center for Global Health and Medicine, 1-7-1, Kohnodai, Ichikawa 272-8516, Japan. Email: mmizokami@hospk.ncgm.go.jp

*JSPS Research Fellow.

Received 14 April 2011; revision 13 June 2011; accepted 15 June 2011.

route of acute hepatitis B in adult is sexual transmission in countries without a universal vaccination program.

Hepatitis B virus genotypes are identified worldwide and classified into at least eight genotypes (A–H) on the basis of a divergence of 8% or more of the entire nucleotide sequences.[1,11–13] In a Japanese population of chronic hepatitis B, the distribution of major HBV genotypes (HBV/A, B, C, and D) was reported to be 1.7%, 12.2%, 84.7%, and 0.4% respectively.[14] However, the prevalence of HBV/A increased to approximately 40% in acute HBV infection, and 4.3% in chronic HBV infection in Japan.[15] The main transmission routes of HBV/A are a contact among men who have sex with men as well as among members of a heterosexual population.[16–19] The expansion of HBV infection has been led by the sexual transmission of HBV/A since little infection by contaminated medical materials has recently been reported in Japan.

As previously reported, phylogenetic analyses based on virus genome revealed the transmission route.[20] The identification of the transmission route provides beneficial information for epidemiologic study and healthcare reform. Although phylogenetic analysis is gradually known in this field, the handlings of the data are difficult to achieve for researchers who are not familiar with genetic analysis. In this study, we have developed a novel computing system to output phylogenetic trees automatically when users simply input their sequence data. The result from this system also shows the type of transmission route such as intrafamilial (mother-to-child, father-to-child, or child-to-child) or horizontal in the general population. For this purpose, sera collected from 10 families with possible intrafamilial transmission were used to reveal their accurate transmission route.

METHODS

Patients

TEN FAMILIES CONSISTING of 23 patients being inactive carriers or having chronic hepatitis B were enrolled in this study after 32 individuals of 10 families

Table 1 Characteristics of intrafamilial transmission cases

Family	Feature	Age	Sex	HBV DNA (Log copies/mL)	Status 1	Status 2	ID
FM1	C	11	F	>9	eAg +	IC	1
	Mo	40	F	8.7	eAg +	IC	2
FM2	C	7	M	>9	eAg +	IC	3
	Mo/S1	41	F	8.6	eAg +	CH	4
	S2	27	F	<2.6	eAb +	IC	5
	S3	30	F	3	eAb +	IC	6
FM3	C	3	F	>9	eAg +	IC	7
	Mo	37	F	>9	eAg +	IC	8
FM4	C1	15	M	>9	eAg +	IC	9
	C2	20	F	>9	eAg +	IC	10
	Mo	47	F	>9	eAg +	IC	11
FM5	C	15	M	5.9	eAb +	IC	12
	Fa	46	M	4.2	eAb +	IC	13
FM6	C	12	M	>9	eAg +	CH	14
	Mo	36	F	>9	eAg +	CH	15
FM7	C	2	F	2.8	eAb +	IC	16
	Mo	33	F	>9	eAg +	IC	17
FM8	C	2	M	>9	eAg +	IC	18
	Mo	41	F	>9	eAg +	IC	19
FM9	C	7	M	3.5	eAb +	IC	20
	Mo	39	F	>9	eAg +	CH	21
FM10	C1	4	M	>9	eAg +	CH	22
	C2	2	F	<2.6	eAb +	IC	23

All patients were hepatitis B surface antigen (HBsAg) positive. Feature: C, children; Mo, mother; Fa, father; S, sister. Sex: M, male; F, female. Status1: Status of HB antigen or antibody except for HbsAg. Status2: IC, inactive carrier; CH, chronic hapatitis. ID 4, 5, 6 are sister and ID 4 is mother of ID 3. ID 22 and 23 are brother and sister.

were tested on HB markers (Table 1). All patients were hepatitis B surface antigen (HBsAg) positive, and the family cases had a possibility of intrafamilial transmission. The histories of familial clustering of HBV infection and hepatitis B vaccination were recorded. The serum samples obtained from all patients were tested for hepatitis B surface antigen (HBsAg), hepatitis B surface antibody (anti-HBs), and hepatitis B core antibody (anti-HBc). Four sera of chronic hepatitis B patients were collected for operation-checks of the developed system before a trial of 23 samples. Serum samples were divided into aliquots and kept at −80 °C until testing. The study protocol conformed to the 1975 declaration of Helsinki and was approved by the ethics committees of the respective institutions. Every patient or his/her next of kin gave informed consent to the purpose of the study. Consent of children for participating in the study was filled by their parents.

Serological testing

Their sera were tested for alanine aminotransferase (ALT), and hepatitis B e antigen (HBeAg) and hepatitis B s antigen (HBsAg), as well as antibodies to HBeAg (anti-HBe) and HBsAg (anti-HBs) (Dinabot, Tokyo, Japan). Antibodies to HBcAg (anti-HBc) were tested by ARCHITECT (Abbott Japan, Tokyo, Japan). The inactive carrier state was defined by the presence of HBV surface antigen (HBsAg) with normal ALT levels over 1 year (examined at least four times at 3-month intervals). Chronic hepatitis was defined by elevated ALT levels (>1.5 times the upper limit of normal [35 IU/L]) persisting over 6 months (with at least three bimonthly tests). HBV DNA levels in sera were quantitated with a commercial kit (Taqman Real-time polymerase chain reaction [PCR] or Amplicor HBV Monitor; Roche Diagnostics, Basel, Switzerland) with a detection range from 2.6 to 9 log copies/mL.

Viral DNA extraction

HBV DNA was extracted from 200 μL of serum using QIAamp DNA Blood Mini Kit (Qiagen, Valencia, CA, USA) according to manufacturer's instruction. The extracted DNA was used for amplification and direct sequencing of S gene as described below.

HBV DNA sequencing

The target of S gene (255 bp, nucleotide positions 458–712) was amplified by nested PCR and sequenced to detect in high sensitivity. The forward primers of S gene were HBS/F2, 5′- AGGTATGTTGCCCGTTTGTC -3′ for the outer set and HBS/F1, 5′- GTATGTTGCCCGTTT GTCCT -3′ for the inner set. The reverse primers of the gene were HBS/R2, 5′- AAAGCCCTACGAACCACTGA −3′ for the outer set and HBS/R1, 5′- AAGCCCTACG AACCACTGAA-3′ for the inner set. Nested PCRs were performed with these primers for 35 cycles (95 °C, 15 s; 58 °C, 30 s; 72 °C, 30 s) in 1st and 2nd PCR using Veriti (Applied Biosystems, Foster City, CA, USA). The PCR products were sequenced on both strands with the BigDye Terminator V3.1 cycle sequencing kit (Applied Biosystems) with the same primers used for the 2nd PCR. The sequencing products were analyzed with an ABI 3130xl DNA analyzer (Applied Biosystems). The obtained sequences were aligned with GenBank sequences corresponding to HBV genotypes.

Database and the system for phylogenetic analysis

The determination of transmission routes using phylogenetic analyses is considered based on age difference, mutation rate, clinical background, and the amplicon size between queries. The determination of non-intrafamilial transmission between queries was performed using a significance level of $P < 10^{-99}$. The criterion was calculated by the simulation of random sampling from Hepatitis Virus Database (HVDB) and the genetic factors described above. The presently developed system, the easy-to-use phylogenetic analysis system (E-PAS) for the determination of genotypes and/or transmission route is implemented in the account mode of the HVDB (http://s2as02.genes.nig.ac.jp). We recommend that researchers contact the web master before use.

Table 2 Reference data for the analysis of transmission root

Genotype	Country	Number of references
A	Foreign	2
B	Japan	24
C	Japan	64
D	Japan	1
E	Foreign	1
F	Foreign	1
G	Foreign	1
H	Japan	3